LiteBIRD Sensitivity Calculation
Version 22

Charles Hill
with Tomotake Matsumura, Aritoki Suzuki,
Kam Arnold, Johannes Hubmayr,
Yuto Minami and Takashi Hasebe

2016-12-21

Revision History

New in Version 22

- Modified the equation for mirror efficiency
- Added the comment for the sapphire index in Table 18

New in Version 21

- Careful readthrough of text, getting ready to hand off to Tomo, Yuto, and Takashi
- Updating tables, figures, and text to represent what we presented in the CSR

New in Version 20

- Updated sensitivity values
- Updated detector count, wafer distributions, optical element assumptions, NEP values, NET margin, etc.
- This version essentially syncs up with the CSR

New in Version 11

- Modification to the extreme loading scenarios from a baffle temperature of 4.5K and 6.0K (formerly 1.5K and 6.0K)
- Introduction of Section 9.2 which plots both band-by-band and overall sensitivity vs the temperature of various optical elements

New in Version 10

- Bug fix in TeX table handling that has changed the following items
  - Table 1: Public vs this document
  - Table 19: Sensitivity with margin

New in Version 9

- Bolometer thermal carrier changed from electron to phonon
- Band center frequencies rounded to nearest GHz

- Upgrades to pixel diameter optimization
  - Presentation of pixel optimization for both reflection to baffle and reflection to focal plane
  - More transparent explanations behind pixel number quantization and limits on pixel size for each frequency band
- Added Section 9.1 to show range of possible in-band loading values for each frequency channel

New in Version 8

- Comparision of public in-band loading vs that of this document
- Explicit list of differences between public sensitivity calculation and that of this document
- Minor bug fix in handling of HFT reflections

New in Version 7

- Added "Opening Remark" that presents the public uK-armin values from Tomo's LTD proceeding adjacent to the uK-arcmin values calculated in this document

New in Version 6

- Explicit calculation of frequency dependencies in the system
- Explicit handling of reflections landing on temperatures other than that of the focal plane
- Transparent presentation of all assumptions behind emissivity and efficiency values of every optical element

Contents

1 Experimental Design Overview 6
- 1.1 Observing Parameters 6
- 1.2 Low Frequency Telescope Focal Plane Specifications 6
- 1.3 High Frequency Telescope Focal Plane Specifications 8
- 1.4 Detector Parameters 9

2 Overview of Noise Sources 10
2.1 Internal Noise . . . 10
2.2 External Noise . . . 10

3 LFT Noise Calculation 11
3.1 Optical Element Efficiencies . . . 11
3.2 Internal Noise . . . 11
3.3 External Noise . . . 12
3.4 Total Detector Noise . . . 13

4 HFT Noise Calculation 14
4.1 Optical Elements . . . 14
4.2 Internal Noise . . . 14
4.3 External Noise . . . 15
4.4 Total Detector Noise . . . 15

5 Overall Experimental Sensitivity 16
5.1 Sensitivity With No Margin . . . 16
5.2 Sensitivity With Margin . . . 17

6 Details of Sensitivity Calculation 20
6.1 Optical Power . . . 20
6.2 Photon NEP . . . 21
6.3 Thermal Carrier NEP . . . 21
6.4 Readout NEP . . . 21
6.5 Detector NEP . . . 21
6.6 Detector NET . . . 22
6.7 NET Array . . . 22
6.8 Sensitivity . . . 22

7 Details of Optical Element Calculations 23
7.1 LFT HWP . . . 23
7.1.1 Assumptions . . . 23
7.1.2 Emissivity . . . 23
7.1.3 Efficiency . . . 24
7.2 HFT HWP . . . 24
7.2.1 Assumptions . . . 24
7.2.2 Emissivity . . . 25
7.2.3 Efficiency . . . 25
7.3 Aperture . . . 25
7.3.1 Efficiency . . . 25

7.3.2 Emissivity 26
7.4 LFT Mirrors 26
7.4.1 Assumptions 26
7.4.2 Emissivity 27
7.4.3 Efficiency 27
7.5 HFT Lenses 27
7.5.1 Assumptions 27
7.5.2 Emissivity 28
7.5.3 Efficiency 28
7.6 2 K Filter 28
7.6.1 Assumptions 29
7.6.2 Emissivity 29
7.6.3 Efficiency 29
7.7 LFT Lenslet 29
7.7.1 Assumptions 30
7.7.2 Emissivity 30
7.7.3 Efficiency 30
7.8 LFT Detector 30
7.8.1 Assumptions 31
7.8.2 Efficiency 31
7.9 HFT Detector 31
7.9.1 Assumptions 31
7.9.2 Efficiency 31

8 Pixel Diameter Optimization 32
8.1 Reflections Go to Baffle, Fixed FOV 32
8.1.1 LF-135 33
8.1.2 LF-246 34
8.1.3 MF-135 Pixel 35
8.1.4 MF-246 36
8.1.5 HFT 37
8.2 Reflections Go to Baffle, Fixed Number of Detectors 38
8.2.1 LF-135 39
8.2.2 LF-246 40
8.2.3 MF-135 41
8.2.4 MF-246 42
8.2.5 HFT 43
8.3 Reflections Go to Focal Plane, Fixed FOV 44
8.3.1 LF-135 45
8.3.2 LF-246 46
8.3.3 MF-135 Pixel 47

8.3.4 MF-246 . . . 48
8.3.5 HFT . . . 49
8.4 Reflections Go to Focal Plane, Fixed Number of Detectors . . . 50
8.4.1 LF-135 . . . 51
8.4.2 LF-246 . . . 52
8.4.3 MF-135 . . . 53
8.4.4 MF-246 . . . 54
8.4.5 HFT . . . 55
8.5 Summary of Optimal Diameters . . . 56
8.6 Choosing Pixel Diameters . . . 57
8.6.1 Hexagon Quantization and Maximum Pixel Diameter . . . 57
8.7 Lenslet Focusing and Minimum Pixel Diameter . . . 58
8.8 Pixel Diameters for this Document . . . 59

9 Discussions 60
9.1 Range of Possible Optical Loading . . . 60
9.2 Effect of Optical Element Temperatures on Sensitivity . . . 62
9.2.1 Effect of Baffle Temperature . . . 63
9.2.2 Effect of HWP Temperature . . . 65
9.2.3 Effect of Aperture Temperature . . . 67
9.2.4 Effect of Mirror/Lens Temperature . . . 69
9.3 Still To Do . . . 71

References 72

1 Experimental Design Overview

This section outlines the basic aspects of the LiteBIRD instrument that are important to our sensitivity estimate.

1.1 Observing Parameters

This document assumes the observing parameters displayed in Table 1.

Parameter	Value
Sky Fraction	1.0
Observing Time	3 years

Table 1: Observing parameters

Note that we take f_{sky} to be 1.0 because LiteBIRD is a full-sky survey.

1.2 Low Frequency Telescope Focal Plane Specifications

Figure 1 is Ted Kisner's drawing of the Low Frequency Telescope (LFT) focal plane, with a color coding scheme to show where each frequency channel lies within the detector array. Table 2 provides the parameters of the frequency channels on the LFT focal plane. Note how the choice pixel size and the fact we are using 6-inch hexagonal wafers determines the number of detectors in each frequency channel.

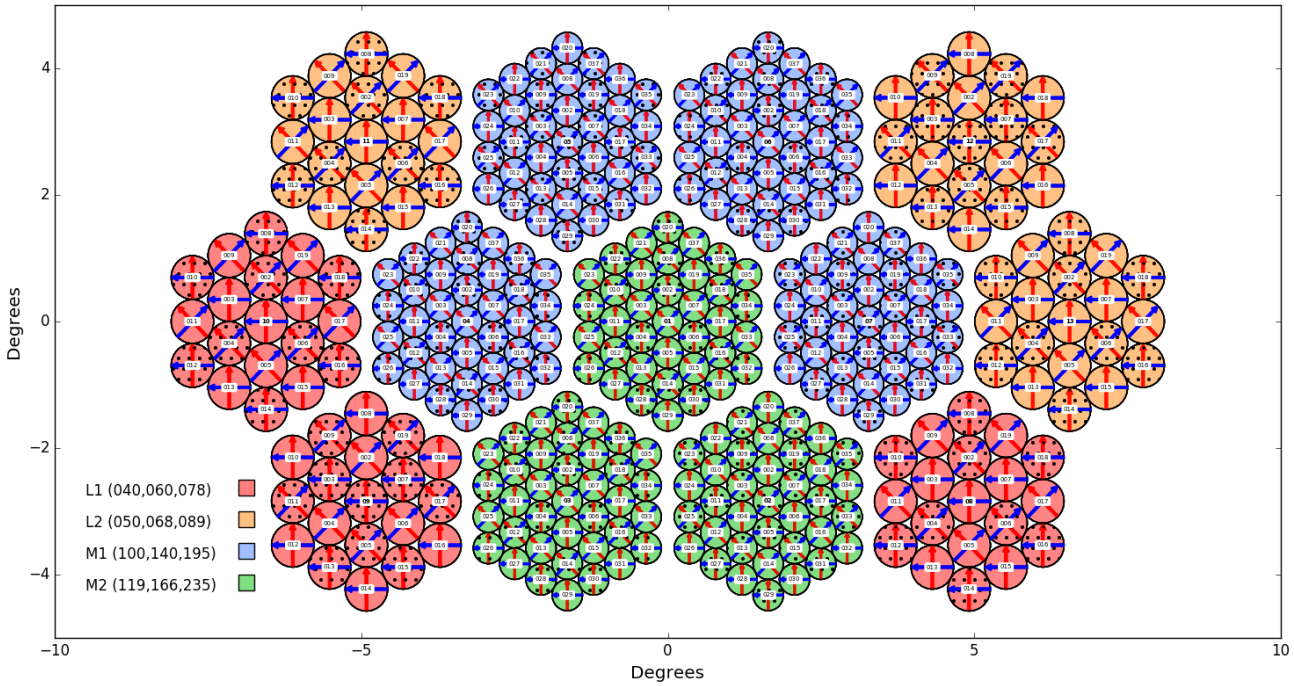

Figure 1: LFT focal plane with wafers color-coded to highlight the location of the corresponding frequency channels

Band	Center Freq [GHz]	Frac BW	Pixel Diameter [mm]	Num Pix	Num Det
LF-1	40	0.30	18	57	114
LF-2	50	0.30	18	57	114
LF-3	60	0.23	18	57	114
LF-4	68	0.23	18	57	114
LF-5	78	0.23	18	57	114
LF-6	89	0.23	18	57	114
MF-1	100	0.23	12	148	296
MF-2	119	0.30	12	111	222
MF-3	140	0.30	12	148	296
MF-4	166	0.30	12	111	222
MF-5	195	0.30	12	148	296
MF-6	235	0.30	12	111	222

Table 2: Frequency channels of the LFT color-coded to highlight the position of each channel on the focal plane

1.3 High Frequency Telescope Focal Plane Specifications

The High Frequency Telescope (HFT) focal plane is an array of monochroic, horn-coupled, orthomode transducers (OMTs) covering three frequencies shown by Hannes Hubmayr's drawing in Figure 2. The parameters of each frequency channel are given in Table 3. For the HFT, while the pixel sizes are optimized (see Section 8), the number of detectors is not at the moment. In other words, we may be able to add more detectors by packing the focal plane more densely. Whether or not this is possible or advisable relies on telemetry and crosstalk requirements.

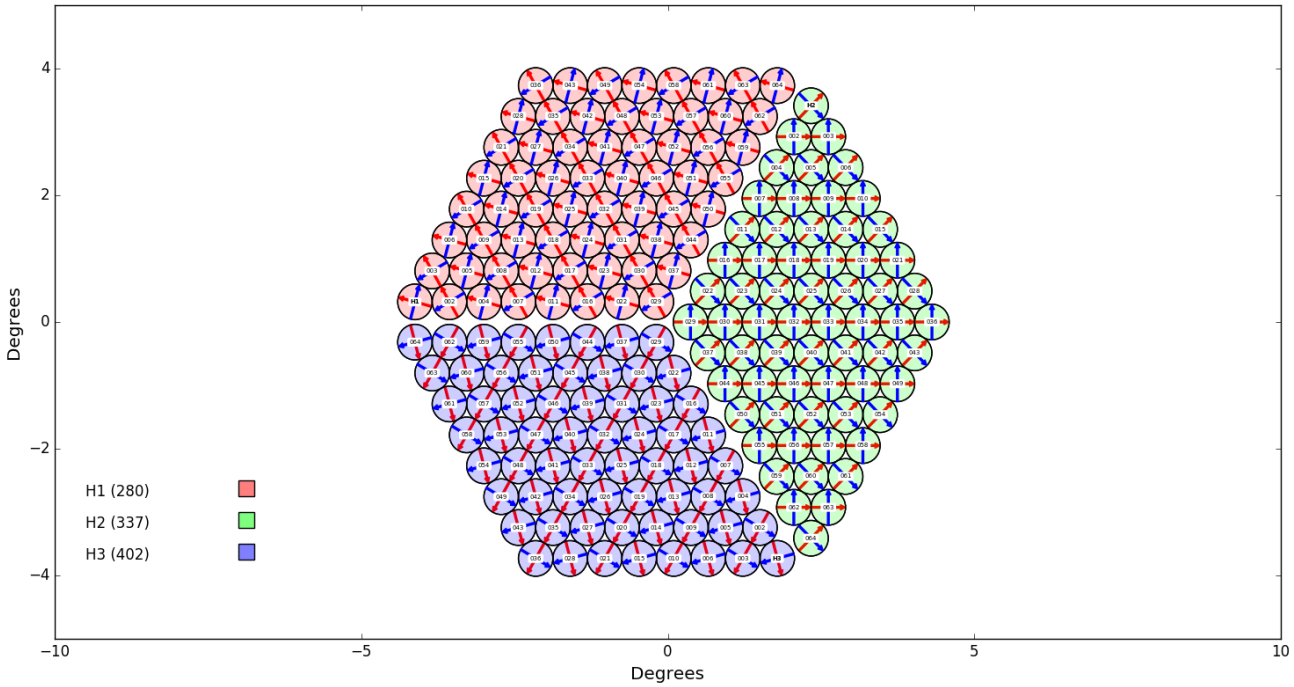

Figure 2: HFT focal plane with detectors color-coded to highlight the location of the corresponding frequency channels

Band	Center Freq [GHz]	Frac BW	Pixel Diameter [mm]	Num Pix	Num Det
HF-1	280	0.30	5.4	64	128
HF-2	337	0.30	4.5	64	128
HF-3	402	0.23	4.0	64	128

Table 3: Frequency channels of the HFT

1.4 Detector Parameters

Table 4 shows the assumptions that we take regarding detector design when calculating noise performance.

Parameter	Assumed Value
Bath Temperature [K]	0.100
Transition Temperature [K]	0.171
Thermal Carrier	Phonon (n = 3)
P_{oper}/P_{opt}	2.5

Table 4: Table of detector parameters

Note that P_{oper} is the operating power of the bolometer and is calculated as

$$P_{oper} = P_{opt} + P_{elec} \tag{1}$$

where P_{opt} and P_{elec} are the optical power and electrical power on the bolometer, respectively.

2 Overview of Noise Sources

For LiteBIRD, we consider two categories of noise sources: internal and external.

2.1 Internal Noise

Internal noise sources are those which are inhrently tied to the fundamental operation of the detector and optics and therefore cannot be easily reduced without changes to the experimental design. The internal noise sources considered in this memo are listed in Table 5.

Internal Noise Source	Symbol	Description
Photon Noise	$\mathrm{NEP_{ph}}$	Noise due to the distrubution of arrival times of photons at the detector input [9]
Thermal Carrier Noise	$\mathrm{NEP_{g}}$	Thermal noise associated with heat transport across the bolometer legs
Readout Noise	$\mathrm{NEP_{read}}$	Noise associated with fluctuations in the bias current across the bolometer

Table 5: Internal Noise Sources

2.2 External Noise

External noise sources are those which interfere with the operation of the designe instrument and can in principle be reduced. The external noise sources considered in this memo are listed in Table 6.

External Noise Source	Symbol	Description
Vibrational Noise	$\mathrm{NEP_{vib}}$	Microphonic noise due to vibrations of the focal plane
Thermal Fluctuation	$\mathrm{NEP_{TF}}$	Noise due to fluctuations in bath temperature
Cosmic Rays	$\mathrm{NEP_{CR}}$	Noise due to TES heating caused by cosmic ray hits
Magnetic Interference	$\mathrm{NEP_{mag}}$	Noise due to magnetic flux fluctuations across the TES
Electromagnetic Interference	$\mathrm{NEP_{EMI}}$	Noise due to electromagnetic interference within the readout system

Table 6: External Noise Sources

It is a requirement that the external noise be subdominant to the internal noise.

3 LFT Noise Calculation

In this section, we overview the optical elements of the LFT and use their specifications to calculate LFT detector noise.

3.1 Optical Element Efficiencies

Table 7 presents the assumed optical parameters for the LFT, with the sky-side-most elements first and the detector-side-most elements last.

Element	T [K]	T_r [K]	ϵ	r	η
CMB	2.725	2.725	1.000	0.000	1.000
HWP	5.000	5.000	$\epsilon_{LFT,HWP}(\nu)$	0.080	$\eta_{LFT,HWP}(\nu)$
Aperture Stop	2.000	NA	$\epsilon_{Aprt}(\nu)$	0.000	$\eta_{Apert}(\nu)$
Primary Mirror	5.000	5.000	$\epsilon_{Mirr}(\nu)$	$r_{Mirr}(\nu)$	$\eta_{Mirr}(\nu)$
Secondary Mirror	5.000	5.000	$\epsilon_{Mirr}(\nu)$	$r_{Mirr}(\nu)$	$\eta_{Mirr}(\nu)$
2 K Filter	2.000	0.100	$\epsilon_{2KF}(\nu)$	0.050	$\eta_{2KF}(\nu)$
Lenslet	0.100	0.100	$\epsilon_{Lenslet}(\nu)$	0.050	$\eta_{Lenslet}(\nu)$
Detector	0.100	0.100	0.000	0.320	0.680

Table 7: LFT optical elements

where T is the temperature of the element, T_r is the temperature the element reflects/scatters to, ϵ is the emissivity of the element, r is the reflectivity of the element, and η is the efficiency of the element. Note that the frequency-dependent values are calculated for each frequency band. **The assumptions and details behind these values can be reviewed in Section 7**.

3.2 Internal Noise

Table 8 presents the calculated internal noise values for the LFT given the assumptions previously presented.

Band	η_{Apert}	P_{opt} [pW]	NEP_{ph} [aW/$\sqrt{Hz}$]	NEP_{g} [aW/$\sqrt{Hz}$]	NEP_{read} [aW/$\sqrt{Hz}$]	NEP_{int} [aW/$\sqrt{Hz}$]
LF-1	0.29	0.15	3.37	2.80	3.27	5.47
LF-2	0.42	0.18	3.98	3.07	3.46	6.10
LF-3	0.54	0.16	4.00	2.89	3.12	5.84
LF-4	0.63	0.17	4.39	3.03	3.02	6.13
LF-5	0.73	0.19	4.84	3.18	3.08	6.56
LF-6	0.82	0.20	5.29	3.29	3.04	6.93
MF-1	0.62	0.18	5.11	3.07	3.67	7.00
MF-2	0.74	0.25	6.47	3.63	4.09	8.47
MF-3	0.85	0.25	7.01	3.66	4.06	8.89
MF-4	0.93	0.24	7.42	3.60	3.94	9.14
MF-5	0.97	0.22	7.59	3.43	3.98	9.23
MF-6	0.99	0.18	7.49	3.10	4.03	9.06

Table 8: LFT internal noise source calculations

3.3 External Noise

Table 9 presents the calculated external noise values for the LFT. **As of 2016-12-20 these have not been calculated**.

Band	NEP_{vib} [aW/$\sqrt{Hz}$]	NEP_{CR} [aW/$\sqrt{Hz}$]	NEP_{TF} [aW/$\sqrt{Hz}$]	NEP_{mag} [aW/$\sqrt{Hz}$]	NEP_{em} [aW/$\sqrt{Hz}$]	NEP_{ext} [aW/$\sqrt{Hz}$]
LF-1						
LF-2						
LF-3						
LF-4						
LF-5						
LF-6						
MF-1						
MF-2						
MF-3						
MF-4						
MF-5						
MF-6						

Table 9: LFT external noise source calculations

It is a requirement that the external noise be subdominant to the

internal noise. Therefore, it is an OK starting point to simply incorporate these values into our contingency when estimating sensitivity.

3.4 Total Detector Noise

Table 10 presents the total detector noise for the LFT by taking the quadrature sum of the internal and external noise sources.

Band	NEP_{int} [aW/$\sqrt{Hz}$]	NEP_{ext} [aW/$\sqrt{Hz}$]	NEP_{det} [aW/$\sqrt{Hz}$]
LF-1	5.47		5.47
LF-2	6.10		6.10
LF-3	5.84		5.84
LF-4	6.13		6.13
LF-5	6.56		6.56
LF-6	6.93		6.93
MF-1	7.00		7.00
MF-2	8.47		8.47
MF-3	8.89		8.89
MF-4	9.14		9.14
MF-5	9.23		9.23
MF-6	9.06		9.06

Table 10: LFT total detector noise calculations

4 HFT Noise Calculation

In this section, we overview the optical elements of the HFT and use their specifications to calculate HFT detector noise.

4.1 Optical Elements

Table 11 presents the assumed optical parameters for the HFT, with the sky-side-most elements first and the detector-side-most elements last. Note that I have called the skyward lens the "objective" and the detector-side lens the "field".

Element	T [K]	T_r [K]	ϵ	r	η
CMB	2.725	2.725	1.000	0.000	1.000
HWP	5.000	5.000	$\epsilon_{HFT,HWP}(\nu)$	0.020	$\eta_{HFT,HWP}(\nu)$
Aperture Stop	2.000	NA	$\epsilon_{Aprt}(\nu)$	0.000	$\eta_{Apert}(\nu)$
Objective Lens	5.000	5.000	$\epsilon_{Lens}(\nu)$	0.020	$\eta_{Lens}(\nu)$
Field Lens	5.000	5.000	$\epsilon_{Lens}(\nu)$	0.020	$\eta_{Lens}(\nu)$
2 K Filter	2.000	0.100	$\epsilon_{2KF}(\nu)$	0.050	$\eta_{2KF}(\nu)$
Detector	0.100	0.100	0.000	0.340	0.660

Table 11: HFT optical elements

where T is the temperature of the element, T_r is the temperature the element reflects/scatters to, ϵ is the emissivity of the element, r is the reflectivity of the element, and η is the efficiency of the element. Note that the frequency-dependent values are calculated for each frequency band. **The assumptions and details behind these values can be reviewed in Section 7**.

4.2 Internal Noise

Table 12 presents the calculated internal noise values for the HFT, given the previously presented assumptions.

Band	η_{Apert}	P_{opt} [pW]	NEP_{ph} [aW/$\sqrt{\text{Hz}}$]	NEP_{g} [aW/$\sqrt{\text{Hz}}$]	NEP_{read} [aW/$\sqrt{\text{Hz}}$]	NEP_{int} [aW/$\sqrt{\text{Hz}}$]
HF-1	0.93	0.13	7.00	2.67	4.15	8.56
HF-2	0.93	0.10	6.49	2.27	4.32	8.12
HF-3	0.95	0.05	5.15	1.64	3.63	6.51

Table 12: HFT internal noise calculations

4.3 External Noise

Table 13 presents the calculated external noise values for the HFT. **As of 2016-12-20 these have not been calculated**.

Band	NEP_{vib} [aW/$\sqrt{Hz}$]	NEP_{TF} [aW/$\sqrt{Hz}$]	NEP_{CR} [aW/$\sqrt{Hz}$]	NEP_{mag} [aW/$\sqrt{Hz}$]	NEP_{EMI} [aW/$\sqrt{Hz}$]	NEP_{ext} [aW/$\sqrt{Hz}$]
HF-1						
HF-2						
HF-3						

Table 13: HFT external noise calculations

It is a requirement that the external noise be subdominant to the internal noise. Therefore, it is an OK starting point to simply incorporate these values into our contingency when estimating sensitivity.

4.4 Total Detector Noise

Table 14 presents the total detector noise for the HFT by taking the quadrature sum of the internal and external noise sources.

Band	NEP_{int} [aW/$\sqrt{Hz}$]	NEP_{ext} [aW/$\sqrt{Hz}$]	NEP_{det} [aW/$\sqrt{Hz}$]
HF-1	8.56		8.56
HF-2	8.12		8.12
HF-3	6.51		6.51

Table 14: HFT total detector noise calculations

5 Overall Experimental Sensitivity

This section summarizes the sensitivity calculations for the LiteBIRD MO design.

5.1 Sensitivity With No Margin

Table 15 presents the LiteBIRD sensitivity assuming no degredation, and Figure 3 presents the sensitivity graphically.

Band	Detector NET $[\mu\mathrm{K}\sqrt{\mathrm{sec}}]$	NET Array $[\mu\mathrm{K}\sqrt{\mathrm{sec}}]$	Sensitivity $[\mu\mathrm{K}-\mathrm{arcmin}]$
LF-1	149	14.0	24.8
LF-2	95.7	8.96	15.9
LF-3	79.1	7.41	13.1
LF-4	64.4	6.03	10.7
LF-5	53.9	5.05	8.95
LF-6	46.7	4.38	7.75
MF-1	58.9	3.42	6.06
MF-2	42.3	2.84	5.03
MF-3	37.8	2.20	3.89
MF-4	36.0	2.42	4.28
MF-5	37.3	2.17	3.84
MF-6	42.8	2.87	5.09
HF-1	54.8	4.92	8.71
HF-2	81.0	7.27	12.9
HF-3	156	14.0	24.8
Total		0.940	1.66
CMB Chans		0.990	1.76

Table 15: LiteBIRD sensitivies with no margin for degradation

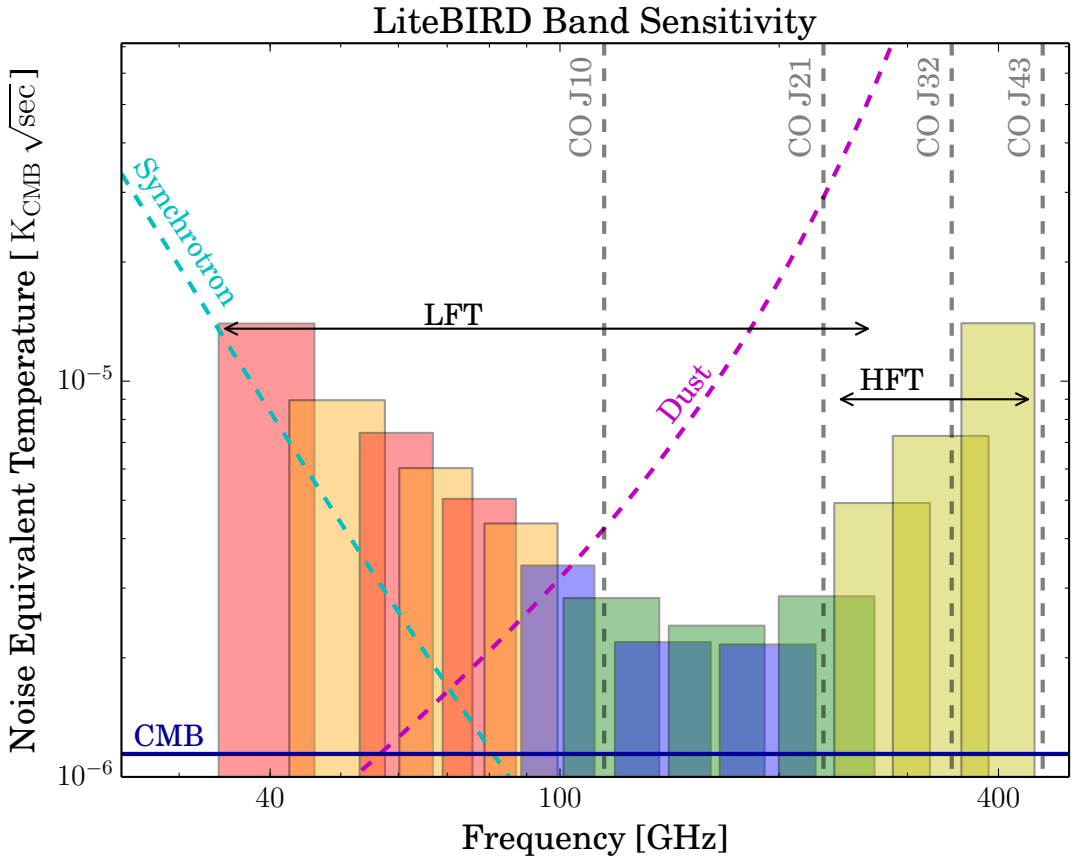

Figure 3: LiteBIRD sensitivity with no margin

5.2 Sensitivity With Margin

We must add safety factors to our calculation to make them viable representations of expected instrumental performance. We add margin to the sensivity calculation using the factors presented in Table 16. Note that the yield and observation time factors were decided prior to the LiteBIRD preproposal by Nils Halverson et al in on 2014-12-11, while the NET margin is floating and is adjusted such that we meet our $\sigma(r = 0) = 5.7 \times 10^{-4}$ requirement.

Parameter	Degredation Factor
Yield	0.8
NET	1.15
Observing Time	0.85 (cosmic ray) $\times$ 0.85 (ADR) = 0.72

Table 16: LiteBIRD degredation factors

Using the factors presented in Table 16, we recalculate experimental sensitivity and present them in Table 17 and Figure 4.

Band	Detector NET $[\mu\mathrm{K}\sqrt{\mathrm{sec}}]$	NET Array $[\mu\mathrm{K}\sqrt{\mathrm{sec}}]$	Sensitivity $[\mu\mathrm{K} - \mathrm{arcmin}]$
LF-1	172	18.0	37.5
LF-2	110	11.5	24.0
LF-3	91.0	9.53	19.9
LF-4	74.1	7.76	16.2
LF-5	62.0	6.50	13.5
LF-6	53.8	5.63	11.7
MF-1	67.8	4.40	9.17
MF-2	48.7	3.65	7.61
MF-3	43.4	2.82	5.88
MF-4	41.4	3.11	6.47
MF-5	42.9	2.79	5.81
MF-6	49.2	3.69	7.70
HF-1	63.0	6.32	13.2
HF-2	93.1	9.35	19.5
HF-3	179	18.0	37.5
Total		1.20	2.51
CMB Chans		1.28	2.66

Table 17: LiteBIRD sensitivies with margin for degradation

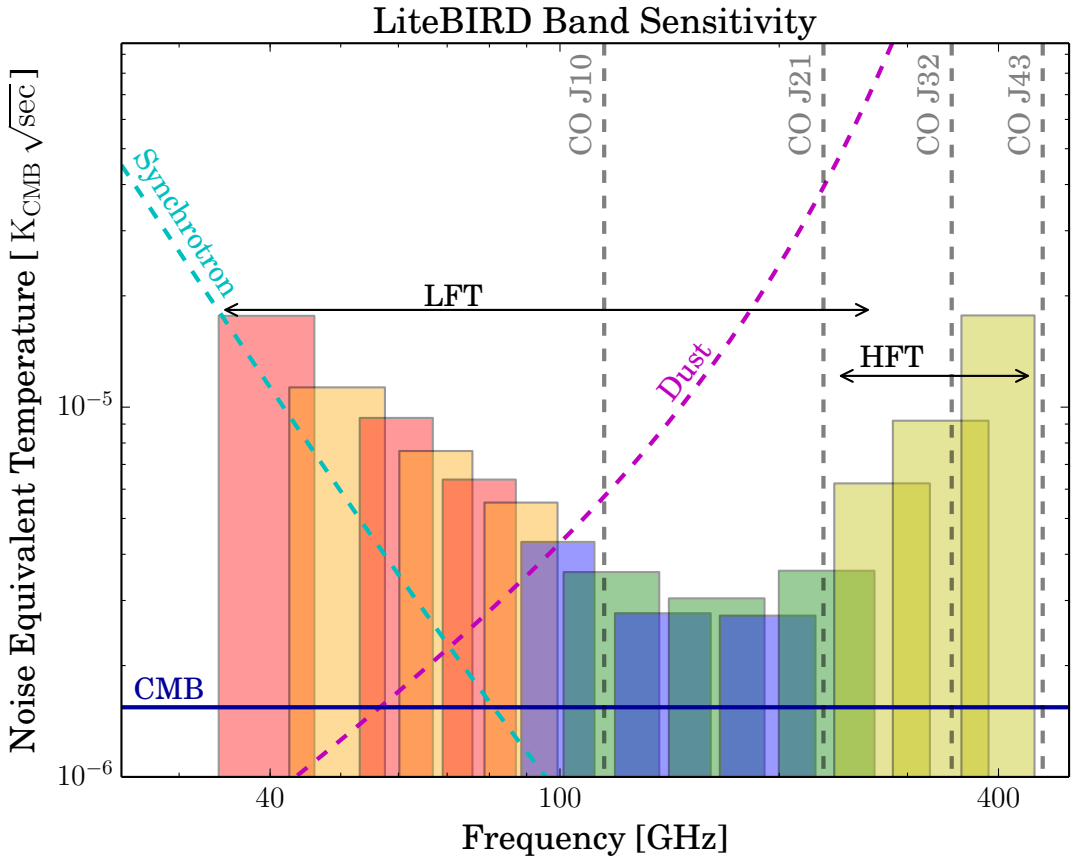

Figure 4: LiteBIRD sensitivity with margin

6 Details of Sensitivity Calculation

This section provides the details of the equations and techniques used to calculate our noise estimates.

6.1 Optical Power

Optical power is calculated via

$$P_{opt} = \int_{\nu_1}^{\nu_2} \Big[\sum_{i=0}^{N_{elem}} P_i(T_i, T_{r;i}, \nu) \Big] \, \mathrm{d}\nu \tag{2}$$

where the summation runs over the optical elements from the sky towards the detector, and where ν_1 and ν_2 are the edges of the band in question. In Equation 2, I've defined

$$P_i(T_i, T_{r;i}, \nu) = E_i(\nu)\, S(T_i, \nu) + R_i(\nu)\, S(T_{r;i}, \nu) \tag{3}$$

where T_i is the temperature of optical element i, $T_{r;i}$ is the temperature that element i reflects to, and $S(T, \nu)$ is the power emitted from a blackbody at temperature T at frequency ν onto a diffraction-limited aperture.

$$S(T, \nu) = \frac{h\,\nu}{e^{\frac{h\nu}{k_B\,T}} - 1} \tag{4}$$

In Equation 3, I've defined

$$E_i = \Big[\prod_{j=i+1}^{N_{elem}} \eta_j(\nu) \Big] \, \epsilon_i(\nu) \tag{5}$$

which is the effective emissivity due to absorption: ϵ_i is the dielectric emissivity of element i, and $\left(\prod_{j=i+1}^{N_{elem}} \eta_j \right)$ represents the cumulative efficiency of everything detector-side of element i. I've also defined

$$R_i = \Big[\prod_{j=i+1}^{N_{elem}} \eta_j(\nu) \Big] \, r_i(\nu) \tag{6}$$

which is the effective emissivity due to reflection: r_i is the reflectivity of element i, and $\left(\prod_{j=i+1}^{N_{elem}} \eta_j \right)$ represents the cumulative efficiency of everything detector-side of element i.

6.2 Photon NEP

We use the following equation to calculate the photon noise equivalent power (NEP) [8]

$$\mathrm{NEP_{ph}} = \sqrt{\int_{\nu_1}^{\nu_2} [\, 2h\nu \sum_{i}^{N_{\mathrm{elem}}} P_i(T_i, T_{r;i}, \nu) + 2\,(\sum_{i}^{N_{\mathrm{elem}}} P_i(T_i, T_{r;i}, \nu))^2\,]\mathrm{d}\nu} \tag{7}$$

where P_i is defined in Equation 3. Notice that we assume 100% photon bunching and that we integrate over the bunching cross terms.

6.3 Thermal Carrier NEP

We use the following equation to calculate thermal carrier noise inherent to the bolometer power dissipation [7]

$$\mathrm{NEP_g} = \sqrt{4k_B P_{oper} T_b \frac{(n+1)^2}{2n+3} \frac{(T_c/T_b)^{2n+3} - 1}{[(T_c/T_b)^{n+1} - 1]^2}} \tag{8}$$

where $T_c = 0.171$ K is the critical temperature, $T_b = 0.100$ K is the bath temperature, $n = 3$ because the thermal carrier is the phonon, and bolometer operation power is calculated as

$$P_{oper} = 2.5\, P_{opt} \tag{9}$$

6.4 Readout NEP

We mandate that the total NEP for each detector be low enough such that we can meet our $\sigma(r = 0)$ requirement. Therefore, NEP_{det} is essentially fixed by the cosmology. To meet this requirement, we float the readout NEP, assuming that we can suppress it with more flexibility than the phton and bolometer noises.

Hence, readout noise is calculated as

$$\mathrm{NEP_{read}} = \sqrt{\mathrm{NEP_{det}^2} - \mathrm{NEP_g^2} + \mathrm{NEP_{read}^2}} \tag{10}$$

6.5 Detector NEP

We find the total detector noise by taking the quadrature sum of the photon, thermal, and readout NEP values

$$\mathrm{NEP_{det}} = \sqrt{\mathrm{NEP_{ph}^2} + \mathrm{NEP_g^2} + \mathrm{NEP_{read}^2}} \tag{11}$$

6.6 Detector NET

We calculate the noise equivalent temperature (NET) of a detector as [8]

$$\mathrm{NET_{det}} = \frac{\mathrm{NEP_{det}}}{\sqrt{2}\,(\mathrm{dP/dT_{CMB}})} \tag{12}$$

where we have defined the conversion factor from power to CMB temperature units as [8]

$$\mathrm{dP/dT_{CMB}} = \int_{\nu_1}^{\nu_2} \Big[\, \frac{\eta}{k_B} \Big(\frac{h\nu}{T_{CMB}(e^{h\nu/k_B T_{CMB}} - 1)} \Big)^2 e^{h\nu/k_B T_{CMB}} \Big] \mathrm{d}\nu \tag{13}$$

where again, ν_1 and ν_2 are the edges of the band. Note that the $\sqrt{2}$ enters because NEP is defined in terms of $1/\sqrt{Hz}$ and NET is defined in terms of $\sqrt{sec}$.

6.7 NET Array

NET Array is calculated as [8]

$$\mathrm{NET_{arr}} = \frac{\mathrm{NET_{det}}}{\sqrt{N_{det}}} \tag{14}$$

where N_{det} is the number of detectors observing in the given frequency band. Note that the unit of NET Array is [K$\sqrt{\mathrm{sec}}$]

6.8 Sensitivity

Sensitivity is calculated as

$$\sigma_S = \sqrt{\frac{4\pi f_{sky}\, 2\, {\mathrm{NET_{arr}}}^2}{t_{obs}}} \Big(\frac{10800}{\pi} \Big) \tag{15}$$

with $f_{sky} = 1.0$ and $t_{obs} = 3$ years $= 94672800$ sec, as defined in Table 1. Note that the factor of $\sqrt{2}$ that accompanies $\mathrm{NET_{arr}}$ accounts for the need of two detectors to measure CMB polarization.

The units of sensitivity are given in K-arcmin.

7 Details of Optical Element Calculations

This section is meant to outline the considerations and assumptions behind the calculation of emissivity, reflection, and efficiency of each optical element in the optical chain of both the LFT and the HFT.

7.1 LFT HWP

This section gives the details behind the calculation of the LFT HWP emissivity, efficiency, and scattering.

7.1.1 Assumptions

Table 18 gives the assumptions for the LFT HWP.

Assumption	Assumed Value	Justification
HWP Material	Sapphire, grooved AR	Discussion with Tomo on 2016-01-14
Sapphire Thickness	$t = 27$ mm	Discussion with Tomo on 2016-01-14. Nine 3mm plates for $\Delta\nu/\nu = 1.55$
Sapphire Index	$n = 3.24$	Page 2019 of [2]. The average of the ordinary and extraordinary axes at 140 GHz and 300 K.
Sapphire Loss Tangent	$\tan\delta = 5 \times 10^{-5}$	Page 2019 of [2] and Fig 2 of [1]
AR Reflection	$r = 0.08$	Discussion with Tomo and Toki on 2016-01-14 gave 10%, pushed to 8% to meet sensitivity requirements
Reflection Temperature	$T_r = 5$ K	100% of scattering goes to 5K baffling

Table 18: LFT HWP assumptions

7.1.2 Emissivity

We calculate the LFT HWP emissivity using the usual equation for absorption [2]

$$\epsilon = 1 - \exp(-2\,\pi\,t\,n\,\tan\delta/\lambda) \tag{16}$$

where the variables t, n, and $\tan\delta$ are defined in Table 18, and λ is the wavelength of the center frequency of the band in question in vacuum.

7.1.3 Efficiency

We calculate the efficiency of the LFT HWP by taking both the reflection and the absorption into account

$$\eta = 1 - r - \epsilon \tag{17}$$

where ϵ is defined in Equation 16, and r is the reflection loss given by the value in Table 18.

7.2 HFT HWP

This section gives the details behind the calculation of the HFT HWP emissivity, efficiency, and scattering.

7.2.1 Assumptions

Table 19 gives the assumptions for the HFT HWP.

Assumption	Assumed Value	Justification
Material	Silicon, grooved AR	Discussion with Tomo on 2016-01-14
Thickness	$t = 4$ mm	Discussion with Tomo on 2016-01-14. Three 1.33 mm plates to give $\Delta\nu/\nu = 0.6$
Index of Refraction	$n = 3.40$	Page 2020 of [2]
Loss Tangent	$\tan\delta = 5 \times 10^{-5}$	Page 2020 of [2] and Fig 2 of [1]
Reflection	$r = 0.02$	Achieved by Jeff McMahon using grooved silicon for $\Delta\nu/\nu = 0.6$
Reflection Temperature	$T_r = 5$ K	100% of scattering goes to 5K baffling

Table 19: HFT HWP assumptions

7.2.2 Emissivity

We calculate the emissivity of the HFT HWP using the usual equation for absorption [2]

$$\epsilon = 1 - \exp(-2\,\pi\,t\,n\,\tan\delta/\lambda) \tag{18}$$

where the variables t, n, and $\tan\delta$ are defined in Table 19, and λ is the wavelength of the center frequency of the band in question in vacuum.

7.2.3 Efficiency

We calculate the efficiency of the HFT HWP by taking both the reflection and the absorption into account

$$\eta = 1 - r - \epsilon \tag{19}$$

where ϵ is defined in Equation 18, and r is the reflection loss given by the value in Table 19.

7.3 Aperture

This section details the calculation of the aperture emissivity and efficiency.

7.3.1 Efficiency

Spillover efficiency is calculated as [7]

$$\eta = 1 - \exp\Big[\frac{\pi^2}{2}\,(\frac{D}{w_0\,F\,\lambda})^2\Big] \tag{20}$$

where F is the F/# of the telescope, D is the pixel diameter, w_0 is the waist ratio, and λ is wavelength of the central frequency of the band in quesion. Values of F, D, and w_0 for the LFT are given in Table 20, and the corresponding values for the HFT are given in Table 21.

LFT Spillover Parameters		
Opitcal Parameter	Assumed Value	Justification
F/#	3.5	Discussions with Tomo on 2016-01-12
Beam Waist Factor D/w_0	2.6	Email correspondance with Tomo on 2015-01-12. Smaller than for PB2 because of many AR layers.

Table 20: LFT frequency-independent optical parameters

HFT Spillover Parameters		
Opitcal Parameter	Assumed Value	Justification
F/#	2.2	Guided by BICEP's refractive optical design [10]
Beam Waist Factor D/w_0	3.1	Taken from an ALMA paper on corrugated horns [11]

Table 21: HFT frequency-independent optical parameters

7.3.2 Emissivity

Because we expect reflection from the aperture to be greatly suppressed, we take the emissivity of the aperture to be the converse of the efficiency.

$$\epsilon = 1 - \eta \tag{21}$$

7.4 LFT Mirrors

This section gives all of the details behind the calculation of the mirror emissivity, efficiency, and scattering.

7.4.1 Assumptions

Table 22 lays out these assumptions behind the mirror calculations.

Assumption	Assumed Value	Justification
Material	Aluminum	Discussion with Tomo and Toki on 2016-01-12
Al Conductivity	$\sigma_c = 36.9$ S/μm	Wikipedia
RMS Roughness	$\sigma_r = 0.2$ μm	Mirror roughness achieved by Planck [6]
Reflection Temperature	$T_r = 5$ K	100% of scattering goes to 5K baffling

Table 22: Mirror assumptions

7.4.2 Emissivity

To calculate the emissivity of the mirror, we take into account the ohmic loss due the finite conductivity of the metal, which is defined to be [3]

$$\epsilon = 4\sqrt{\frac{\pi\nu\mu_0}{\sigma_c}}\frac{1}{Z_0} \tag{22}$$

where ν is the central frequency of the band in question, μ_0 is the permeability of free space, $Z_0 = \sqrt{\mu_0/\epsilon_0}$ is the impedance of free space, and σ_c is the reflector conductivity defined in Table 22.

7.4.3 Efficiency

To calculate the efficiency of the mirror, we consider the ohmic loss

$$\eta = 1 - \epsilon \tag{23}$$

where ϵ is defined in Equation 22.

7.5 HFT Lenses

This section gives the details behind the calculation of the HFT lens emissivity, efficiency, and scattering.

7.5.1 Assumptions

Table 23 lays out the assumptions behind the HFT Lens calculations.

Assumption	Assumed Value	Justification
Lens Material	Silicon, grooved AR	Discussion with Tomo 2016-01-12
Thickness	$t = 20$ mm	Discussion with Tomo 2016-01-14: minimum rigidity needed for safe launch (rough guess)
Silicon Index	$n = 3.40$	Page 2020 of [2]
Silicon Loss Tangent	$\tan\delta = 5 \times 10^{-5}$	Page 2020 of [2] and Fig 2 of [1]
AR Reflection	$r = 0.02$	Achieved by Jeff McMahon using grooved silicon for $\Delta\nu/\nu = 0.6$
Reflection Temperature	$T_r = 5$ K	100% of scattering goes to 5K baffling

Table 23: HFT Lens assumptions

7.5.2 Emissivity

We calculate the emissivity of the HFT lenses using the usual equation for absorption

$$\epsilon = 1 - \exp(-2\,\pi\,t\,n\,\tan\delta/\lambda) \tag{24}$$

where the variables t, n, and $\tan\delta$ are defined in Table 19, and λ is the wavelength of the center frequency of the band in question.

7.5.3 Efficiency

We calculate the efficiency of the HFT lens by taking both the reflection and the absorption into account

$$\eta = 1 - r - \epsilon \tag{25}$$

where ϵ is defined in Equation 24, and r is the reflection loss given by the value in Table 23.

7.6 2 K Filter

This section gives the details behind the calculation of the LFT and HFT 2 K filter emissivity, efficiency, and scattering.

7.6.1 Assumptions

Table 24 lays out these assumptions behind the 2 K Filter calculations.

Assumption	Assumed Value	Justification
Substrate Material	Polypropylene	Cardiff filter design [4]
Substrate Thickness	$t = 5$ mm	Discussion with Tomo 2016-01-12: measuring a spare filter in the UCB lab
Substrate Index	$n = 1.5$	Page 2013 of [2]
Loss Tangent	$\tan\delta = 2.3 \times 10^{-4}$	Page 2013 of [2]
AR Reflection	$r = 0.05$	Discussion with Tomo on 2016-01-14, looking at a plot from [5]
Reflection Temperature	$T_r = 100$ mK	100% of scattering goes to back to focal plane

Table 24: 2 K Filter assumptions

7.6.2 Emissivity

We calculate the emissivity of the HFT lenses using the usual equation for absorption

$$\epsilon = 1 - \exp(-2\,\pi\,t\,n\,\tan\delta/\lambda) \tag{26}$$

where the variables t, n, and $\tan\delta$ are defined in Table 24, and λ is the wavelength of the center frequency of the band in question.

7.6.3 Efficiency

We calculate the efficiency of the HFT lens by taking both the reflection and the absorption into account

$$\eta = 1 - r - \epsilon \tag{27}$$

where ϵ is defined in Equation 26, and r is the reflection loss given by the value in Table 24.

7.7 LFT Lenslet

This section gives the details behind the calculation of the LFT Lenslet emissivity, efficiency, and scattering.

7.7.1 Assumptions

Table 25 lays out these assumptions behind the LFT Lenslet calculations.

Assumption	Assumed Value	Justification
Lenlet Material	Silicon, grooved AR	Discussion with Toki on 2016-01-12
Lenlset Thickness	$t = 9$ mm	Estimated average thickness using LFT pixel radii
Silicon Index	$n = 3.4$	Page 2020 of [2]
Silicon Loss Tangent	$\tan\delta = 5 \times 10^{-5}$	Page 2020 of [2] and Fig 2 of [1]
AR Reflection	$r = 0.05$	Discussion with Toki and Tomo on 2016-01-15
Reflection Temperature	$T_r = 100$ mK	100% of scattering goes to back to focal plane

Table 25: LFT Lenslet assumptions

7.7.2 Emissivity

We calculate the emissivity of the LFT Lenslet using the usual equation for absorption

$$\epsilon = 1 - \exp(-2\,\pi\,t\,n\,\tan\delta/\lambda) \tag{28}$$

where the variables t, n, and $\tan\delta$ are defined in Table 25, and λ is the wavelength of the center frequency of the band in question.

7.7.3 Efficiency

We calculate the efficiency of the HFT lens by taking both the reflection and the absorption into account

$$\eta = 1 - r - \epsilon \tag{29}$$

where ϵ is defined in Equation 28, and r is the reflection loss given by the value in Table 25.

7.8 LFT Detector

This section gives the details behind the calculation of the LFT Detector efficiency.

7.8.1 Assumptions

Table 26 lays out these assumptions behind LFT Detector calculations.

Assumption	Assumed Value	Justification
Reflection/Absorption	$\epsilon = 0.32$	30% estimate from Toki on 2016-01-12, plus an additional 98% optical coupling factor

Table 26: LFT Detector assumptions

7.8.2 Efficiency

We calculate the efficiency of the LFT Detector by taking the converse of the absorption in the on-chip transimssion line

$$\eta = 1 - \epsilon \tag{30}$$

where ϵ is the absorption loss given by the value in Table 26.

7.9 HFT Detector

This section gives the details behind the calculation of the HFT Detector efficiency.

7.9.1 Assumptions

Table 27 lays out these assumptions behind the HFT Detector calculations.

Assumption	Assumed Value	Justification
Reflection/Absorption	$\epsilon = 0.34$	30% conservative estimate from Hannes via email on 2016-01-13, with an additional 96% optical coupling factor

Table 27: HFT Detector assumptions

7.9.2 Efficiency

We calculate the efficiency of the HFT Detector by taking the converse of the absorption in the on-chip OMT

$$\eta = 1 - \epsilon \tag{31}$$

where ϵ is the absorption loss given by the value in Table 27.

8 Pixel Diameter Optimization

We optimize the pixel diamter of both telescopes by maximizing mapping speed for each pixel. Mapping speed is calculated using the following equation [8]

$$\mathrm{MS} \propto \frac{1}{\mathrm{NET_{det}}^2} \quad [\mathrm{K}^{-2}\,\mathrm{sec}^{-1}] \tag{32}$$

To thorougly asses all possible scenarios, we will optimize pixel diameter for the following situations:

- Fixed Field of View (FOV) vs Fixed Detector Number
- All reflections go to baffling vs all reflections go back to the focal plane
- Observation of an extended source vs of a point source

Note that this is not a calculation of pixel spacing, which is determined by number of detectors, the geometry of the wafer, and the fraction of the wafer area that can be occupied by blometers and antennas.

For this section, we will use the naming convention outlined in Table 28 to differentiate pixels on the LFT

LFT Pixel	LFT Detectors
LF-135	LF-1, LF-3, LF-5
LF-246	LF-2, LF-4, LF-6
MF-135	MF-1, MF-3, MF-5
MF-246	MF-2, MF-4, MF-6

Table 28: LFT Pixel naming convention

8.1 Reflections Go to Baffle, Fixed FOV

This subsection containts the results for the optimization of pixel diameters for the LFT and HFT given a fixed field of view and assuming all reflections go to the baffling.

8.1.1 LF-135

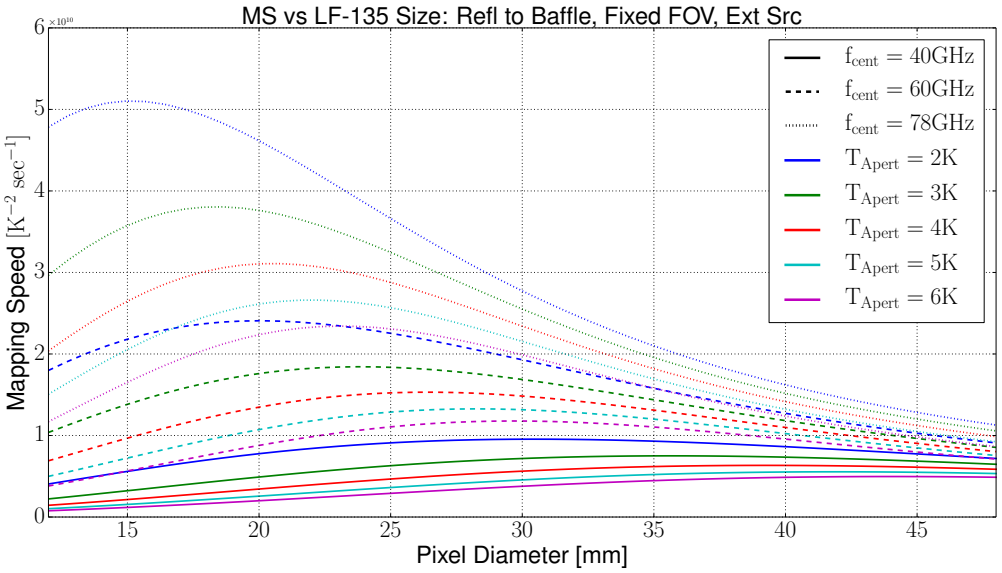

Figure 5: LF-135 mapping speed of an extended source as a function of pixel diameter for hot reflections and fixed FOV

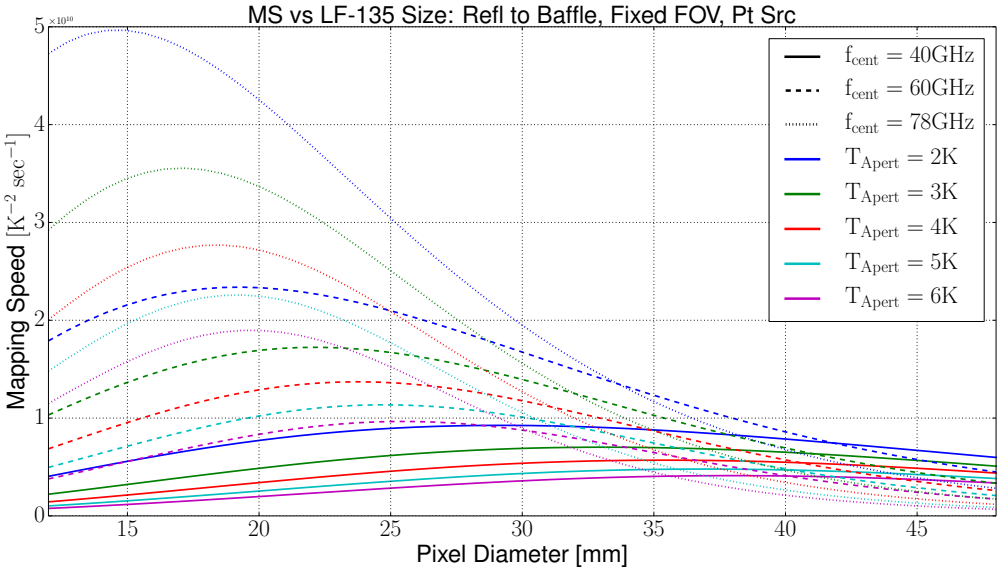

Figure 6: LF-135 mapping speed of a point source as a function of pixel diameter for hot reflections and fixed FOV

8.1.2 LF-246

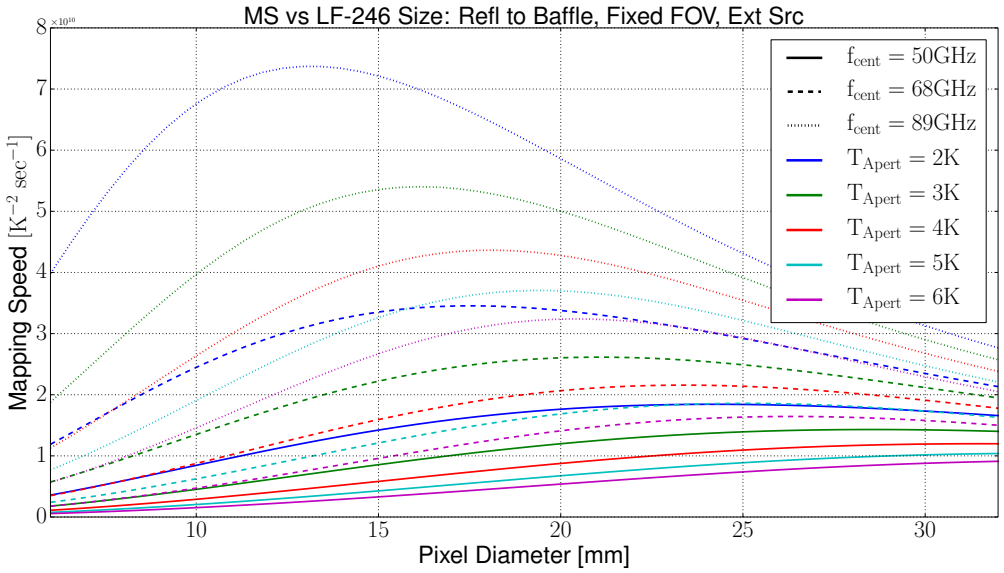

Figure 7: LF-246 mapping speed of an extended source as a function of pixel diameter for hot reflections and fixed FOV

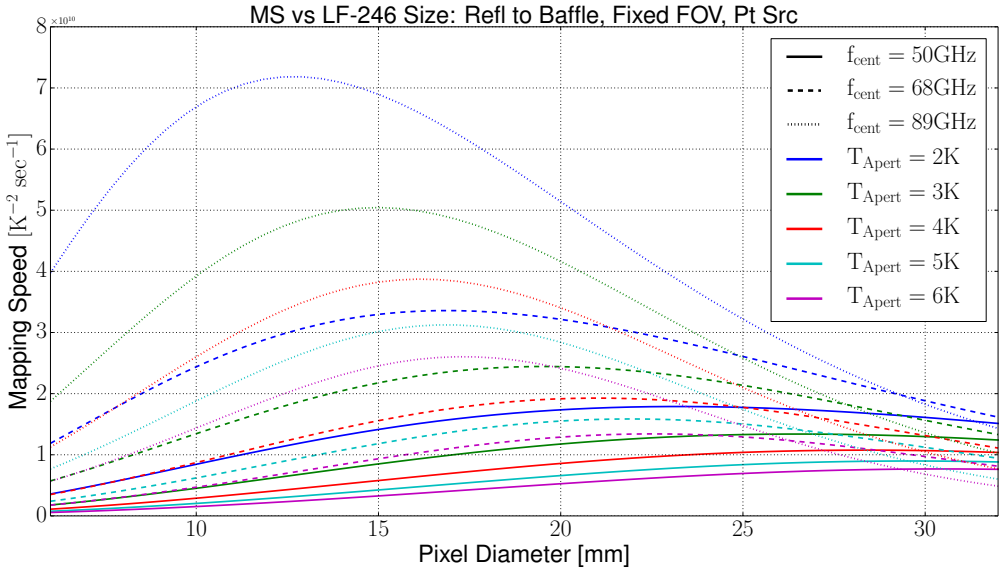

Figure 8: LF-246 mapping speed of a point source as a function of pixel diameter for hot reflections and fixed FOV

8.1.3 MF-135 Pixel

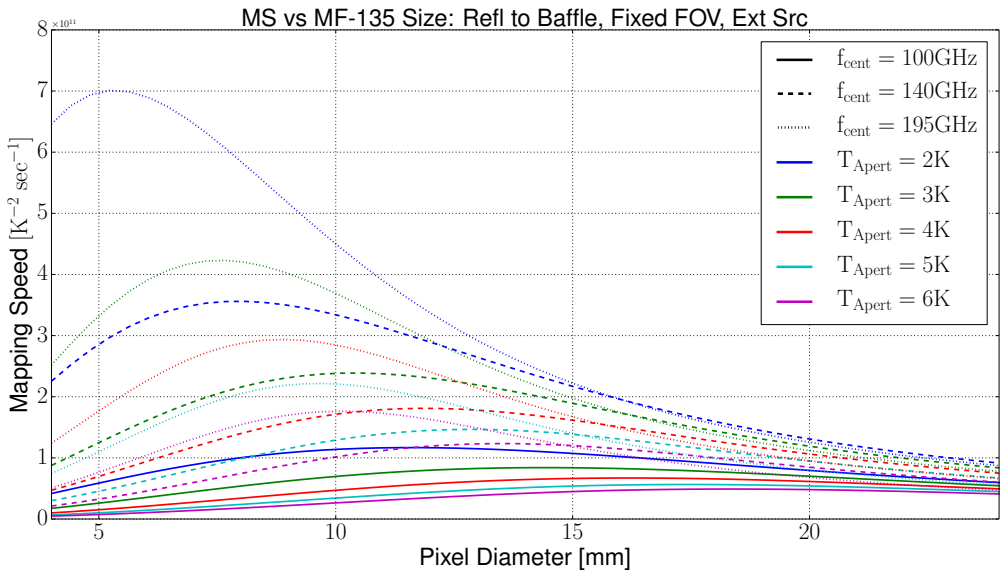

Figure 9: MF-135 mapping speed of an extended source as a function of pixel diameter for hot reflections and fixed FOV

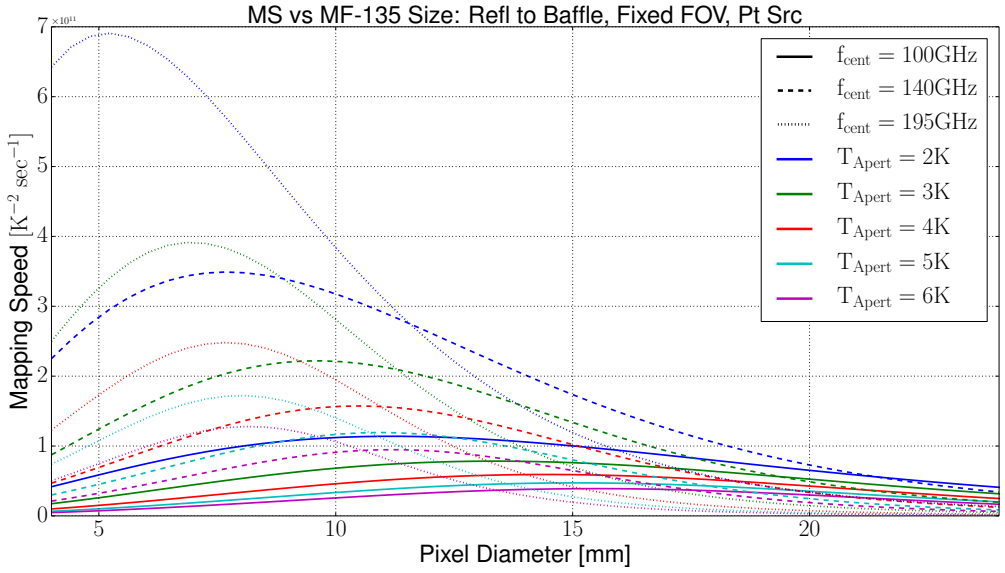

Figure 10: MF-135 mapping speed of a point source as a function of pixel diameter for hot reflections and fixed FOV

8.1.4 MF-246

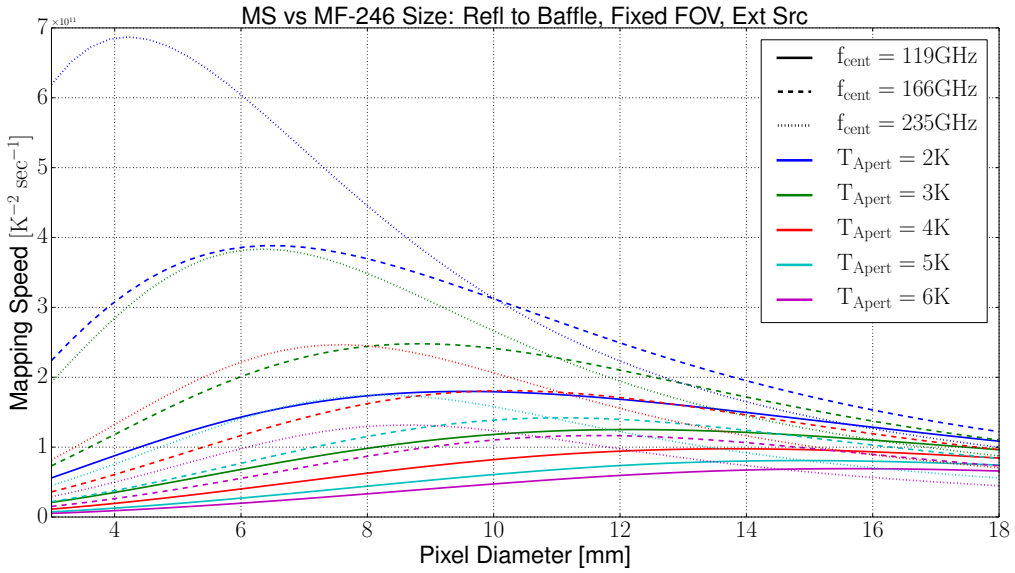

Figure 11: MF-246 mapping speed of an extended source as a function of pixel diameter for hot reflections and fixed FOV

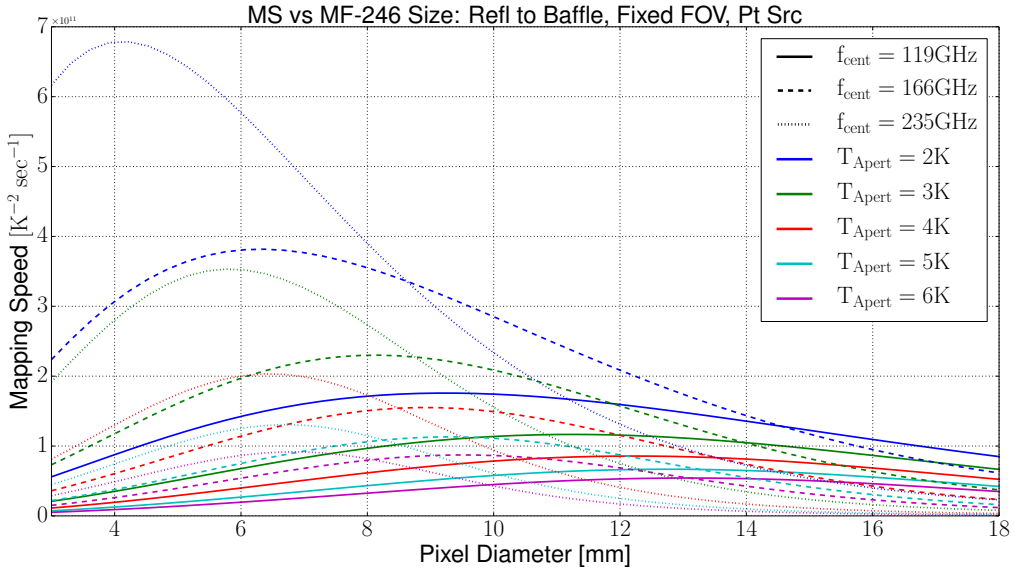

Figure 12: MF-246 mapping speed of a point source as a function of pixel diameter for hot reflections and fixed FOV

8.1.5 HFT

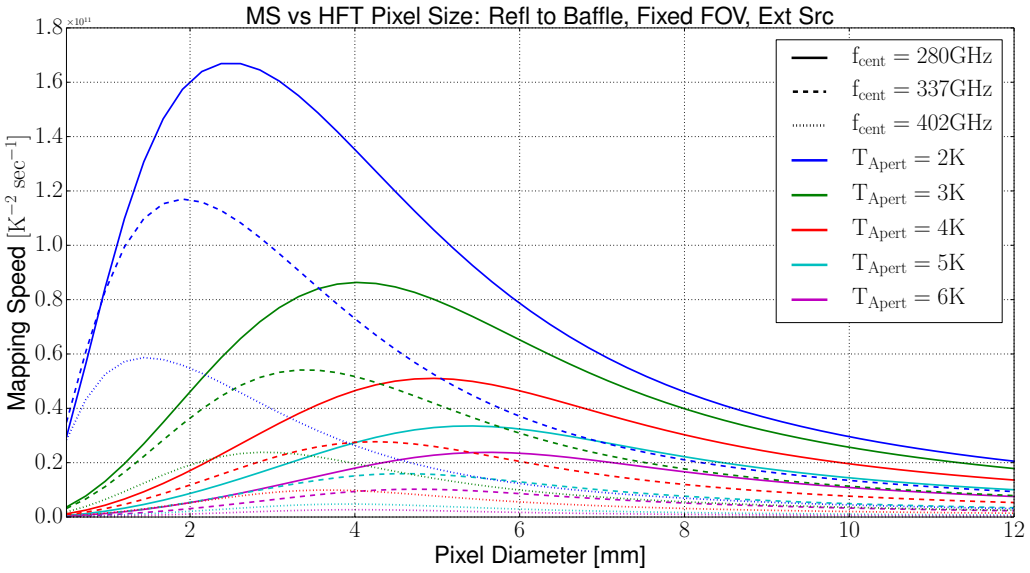

Figure 13: HFT mapping speed of an extended source as a function of pixel diameter for hot reflections and fixed FOV

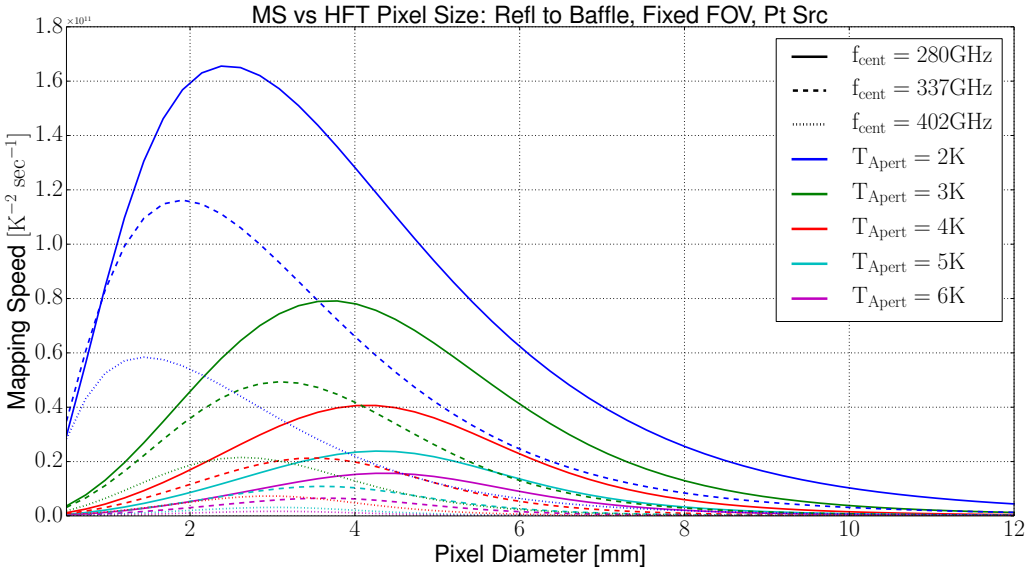

Figure 14: HFT mapping speed of a point source as a function of pixel diameter for hot reflections and fixed FOV

8.2 Reflections Go to Baffle, Fixed Number of Detectors

This subsection containts the results for the optimization of pixel diameters for the LFT and HFT given a fixed number of detectors and assuming all reflections go to the baffling.

8.2.1 LF-135

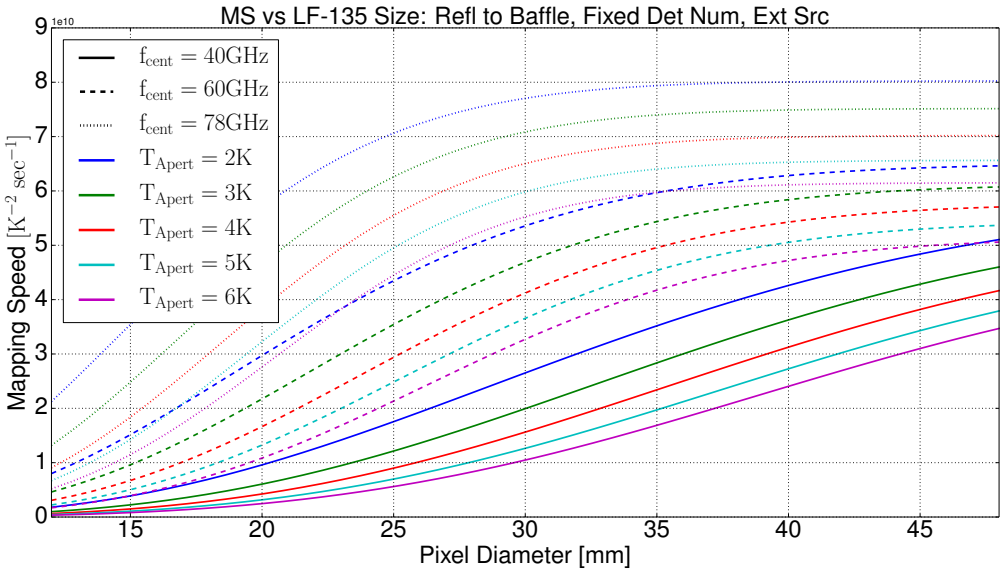

Figure 15: LF-135 mapping speed of an extended source as a function of pixel diameter for hot reflections and fixed number of detectors

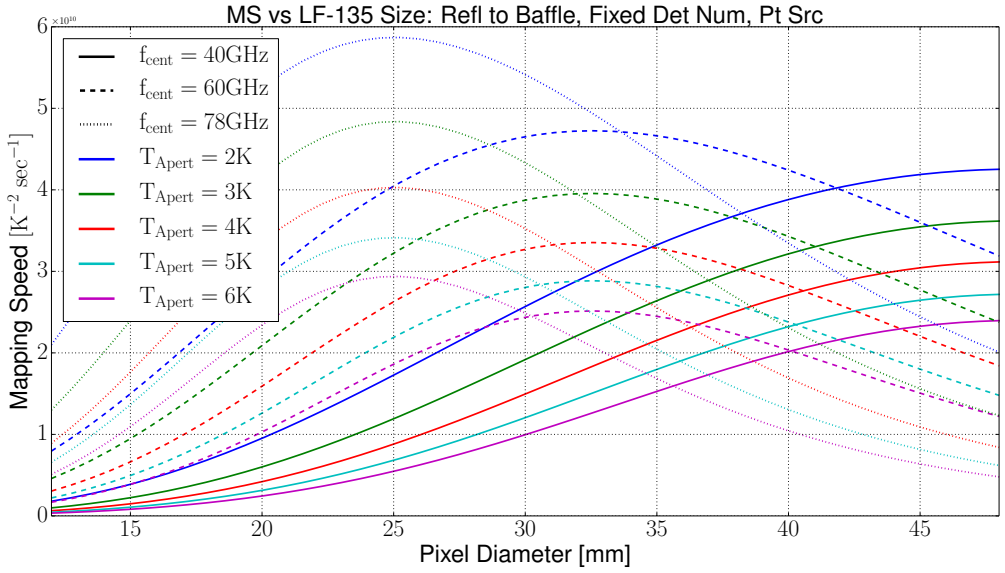

Figure 16: LF-135 mapping speed of a point source as a function of pixel diameter for hot reflections and fixed number of detectors

8.2.2 LF-246

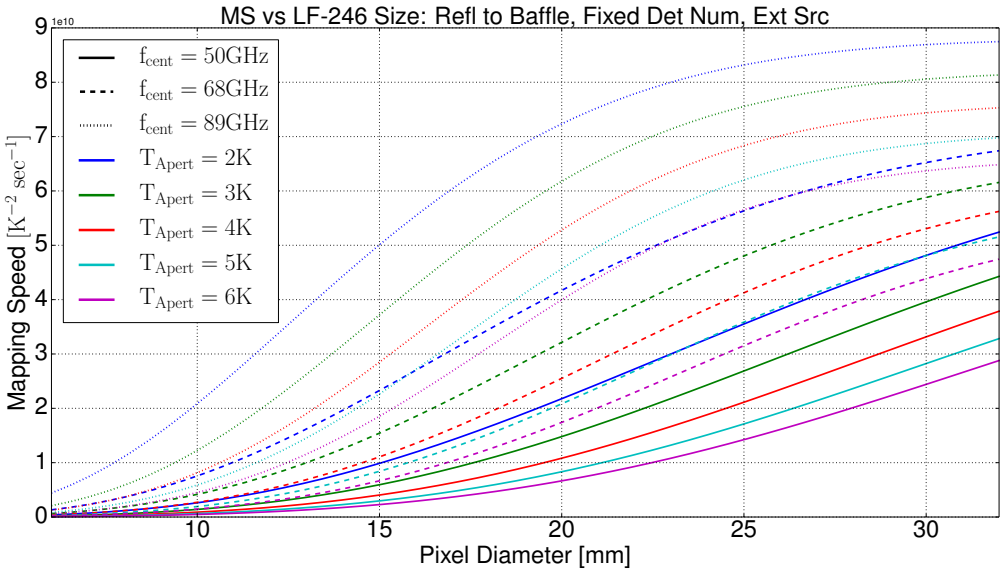

Figure 17: LF-246 mapping speed of an extended source as a function of pixel diameter for hot reflections and fixed number of detectors

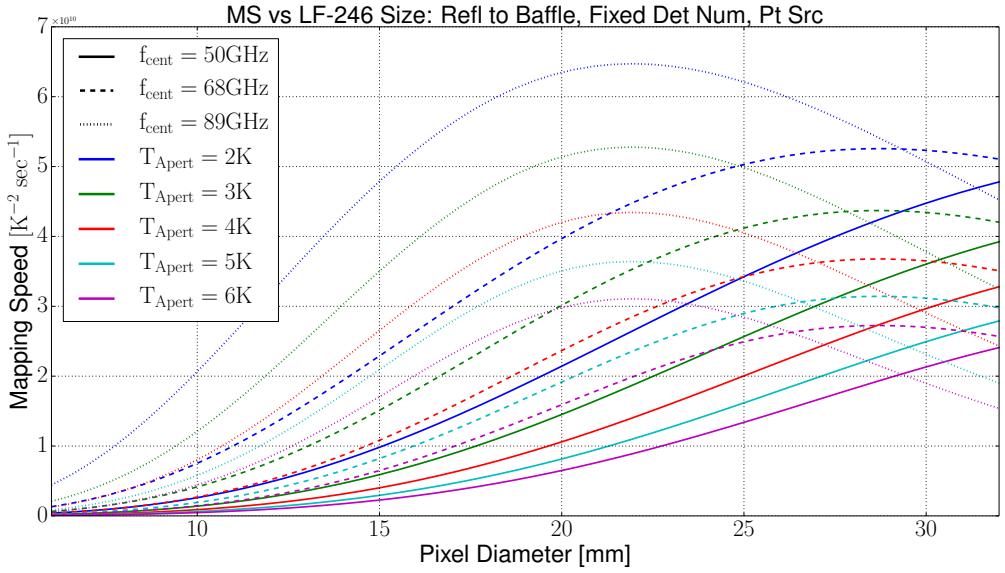

Figure 18: LF-246 mapping speed of a point source as a function of pixel diameter for hot reflections and fixed number of detectors

8.2.3 MF-135

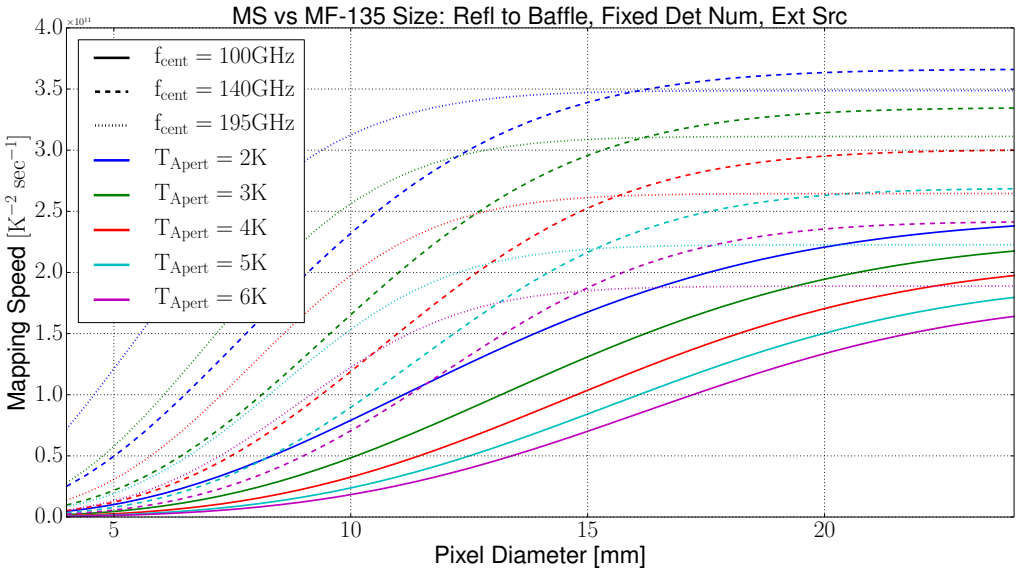

Figure 19: MF-135 mapping speed of an extended source as a function of pixel diameter for hot reflections and fixed number of detectors

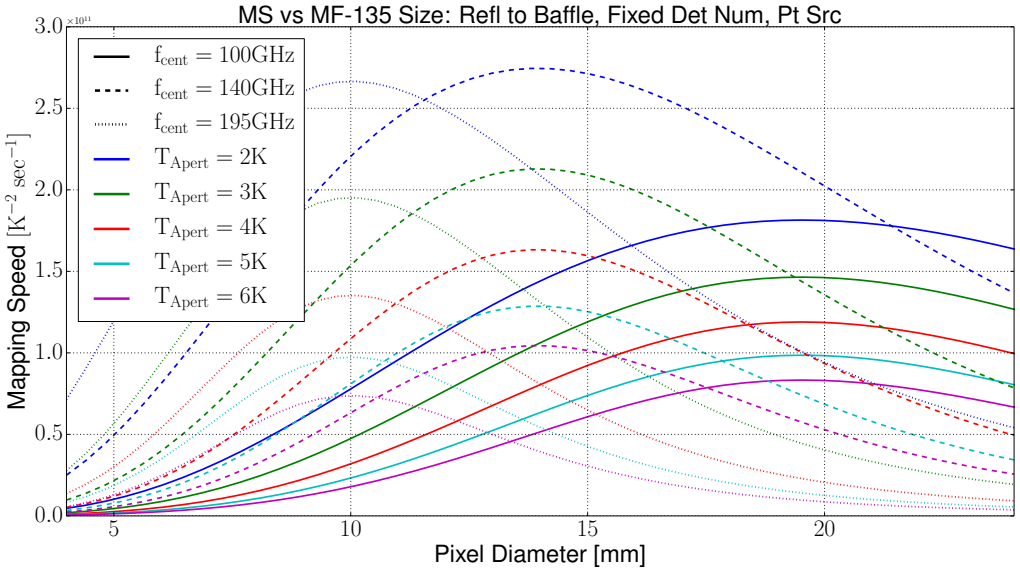

Figure 20: MF-135 mapping speed of a point source as a function of pixel diameter for hot reflections and fixed number of detectors

8.2.4 MF-246

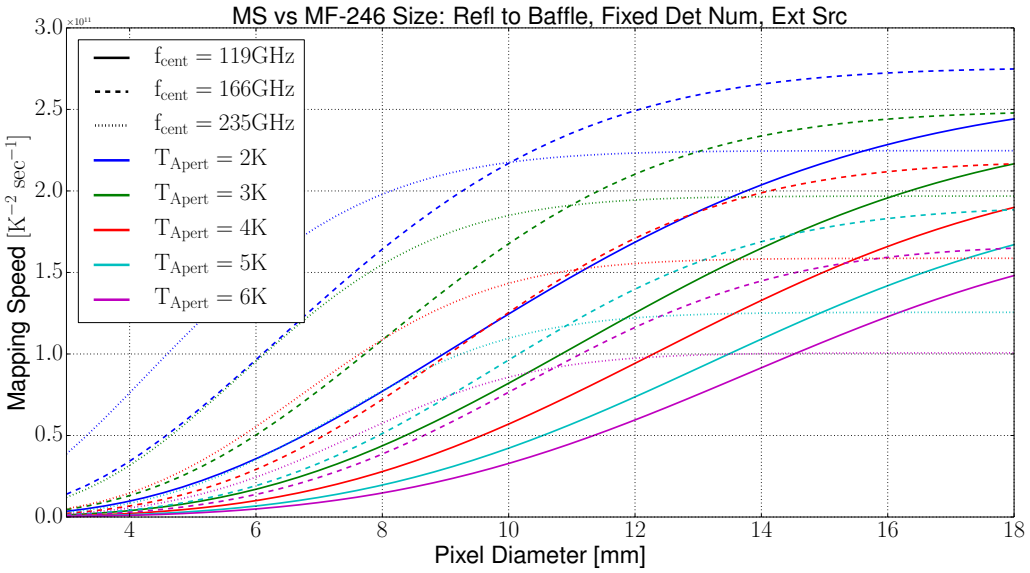

Figure 21: MF-246 mapping speed of an extended source as a function of pixel diameter for hot reflections and fixed number of detectors

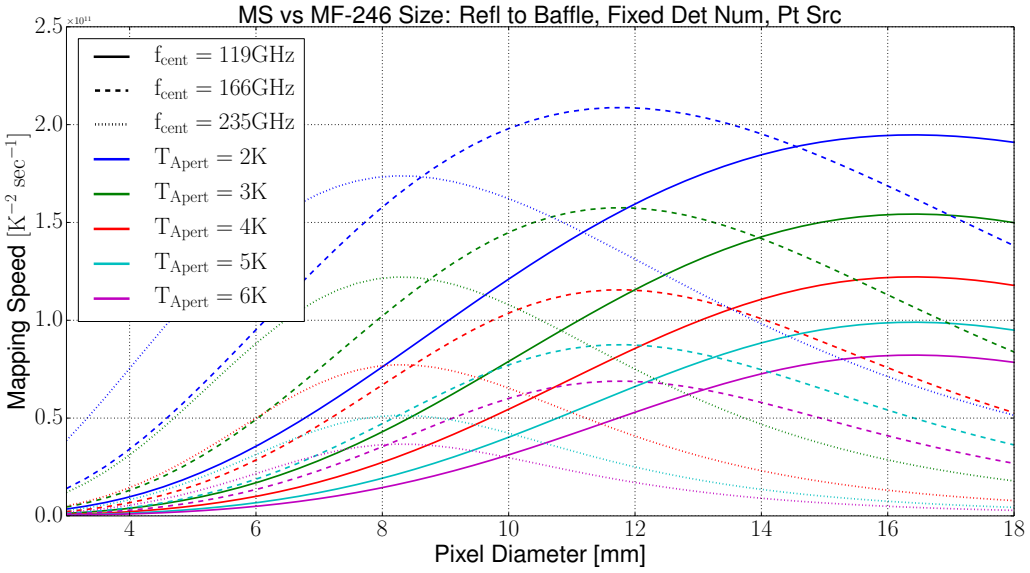

Figure 22: MF-246 mapping speed of a point source as a function of pixel diameter for hot reflections and fixed number of detectors

8.2.5 HFT

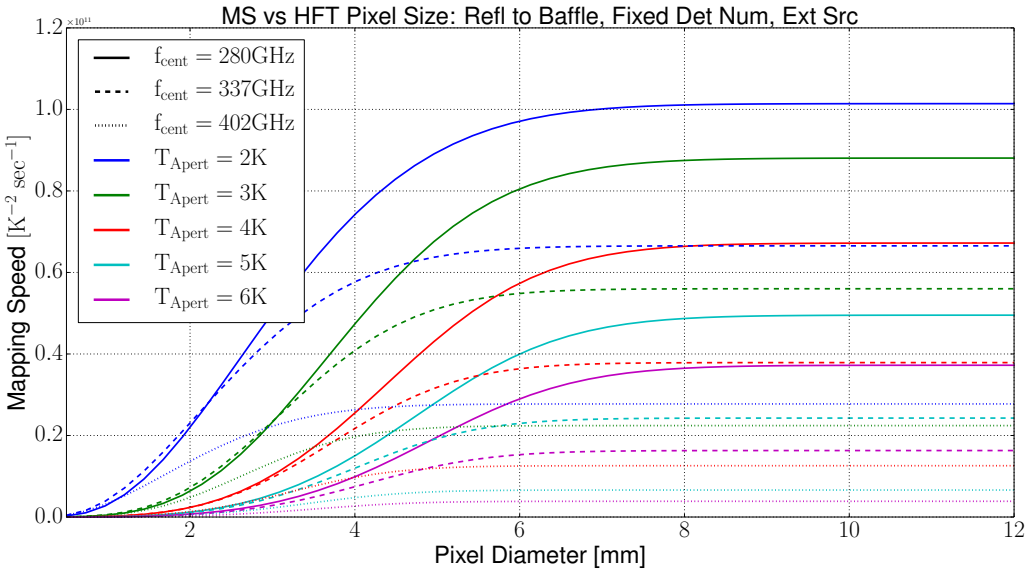

Figure 23: HFT mapping speed of an extended source as a function of pixel diameter for hot reflections and fixed number of detectors

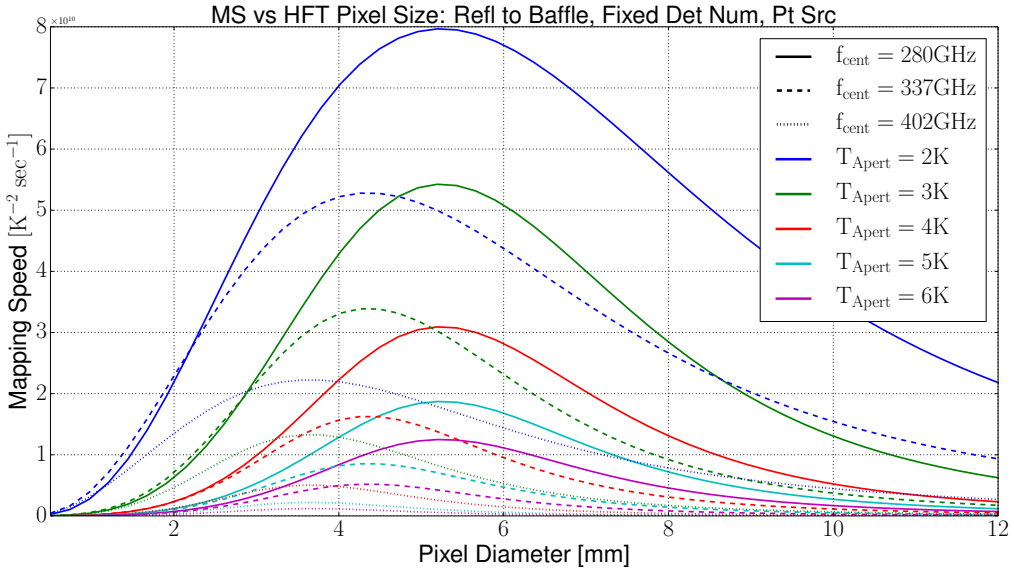

Figure 24: HFT mapping speed of a point source as a function of pixel diameter for hot reflections and fixed number of detectors

8.3 Reflections Go to Focal Plane, Fixed FOV

This subsection containts the results for the optimization of pixel diameters for the LFT and HFT given a fixed field of view and assuming all reflections go back to the focal plane.

8.3.1 LF-135

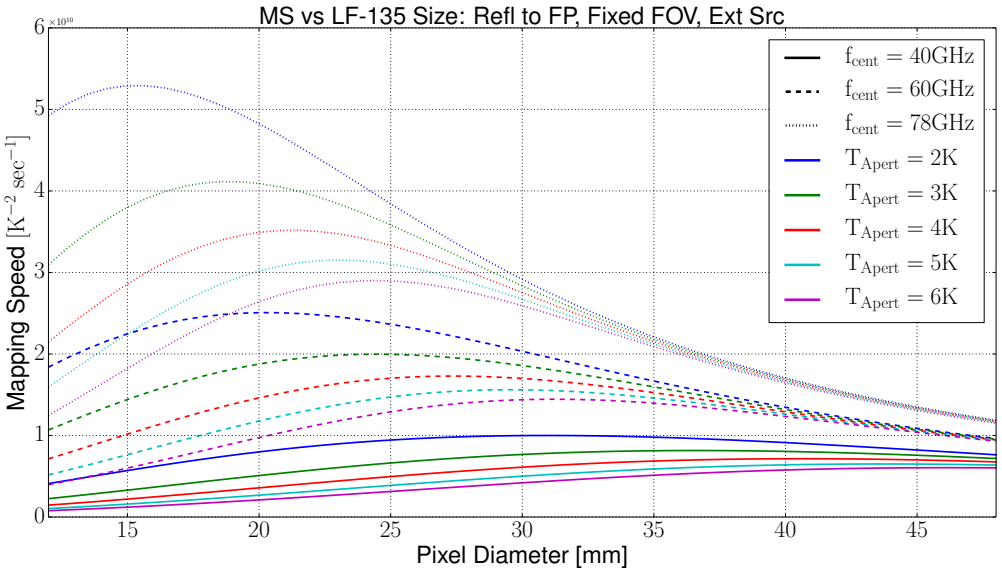

Figure 25: LF-135 mapping speed of an extended source as a function of pixel diameter for cold reflections and fixed FOV

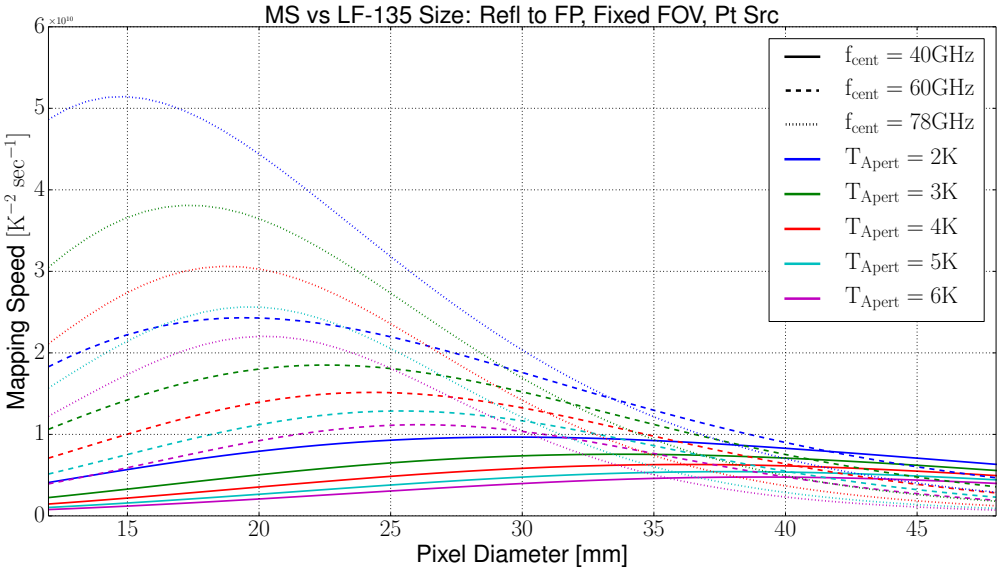

Figure 26: LF-135 mapping speed of a point source as a function of pixel diameter for cold reflections and fixed FOV

8.3.2 LF-246

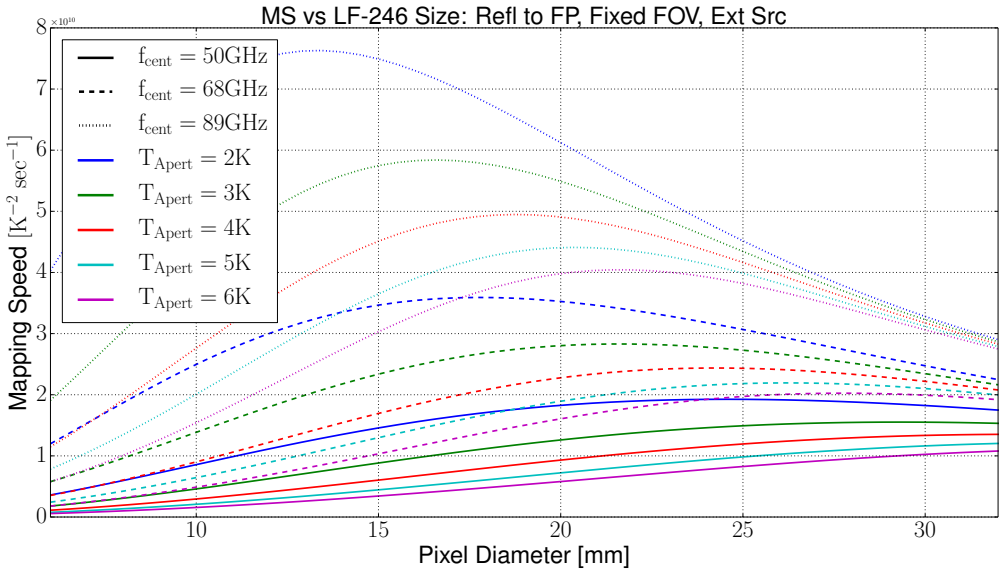

Figure 27: LF-246 mapping speed of an extended source as a function of pixel diameter for cold reflections and fixed FOV

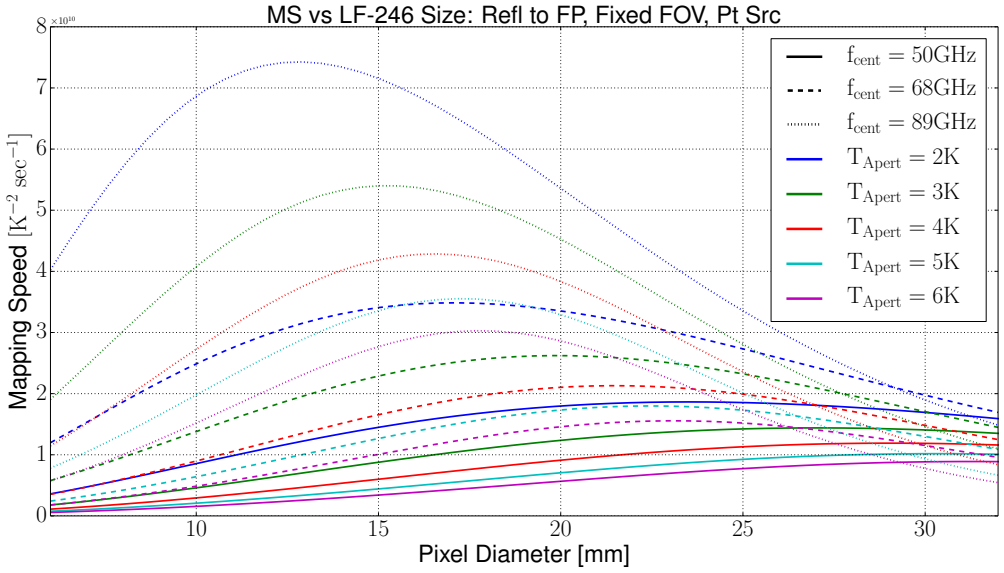

Figure 28: LF-246 mapping speed of a point source as a function of pixel diameter for cold reflections and fixed FOV

8.3.3 MF-135 Pixel

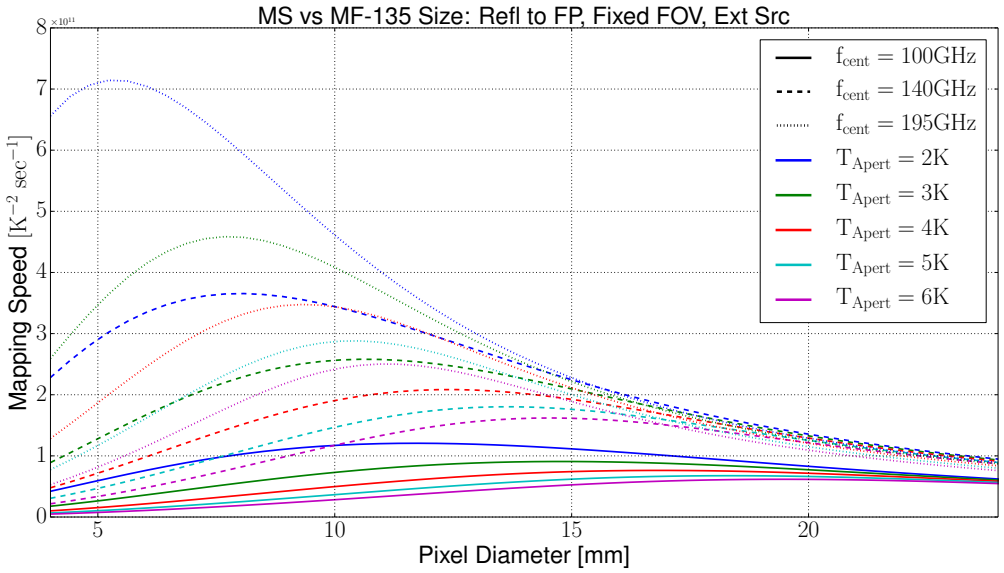

Figure 29: MF-135 mapping speed of an extended source as a function of pixel diameter for cold reflections and fixed FOV

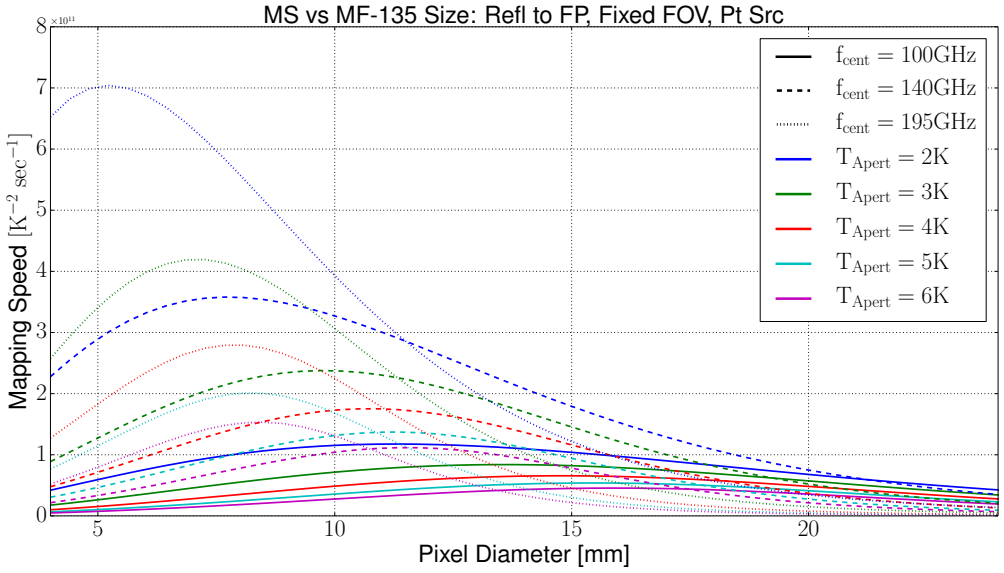

Figure 30: MF-135 mapping speed of a point source as a function of pixel diameter for cold reflections and fixed FOV

8.3.4 MF-246

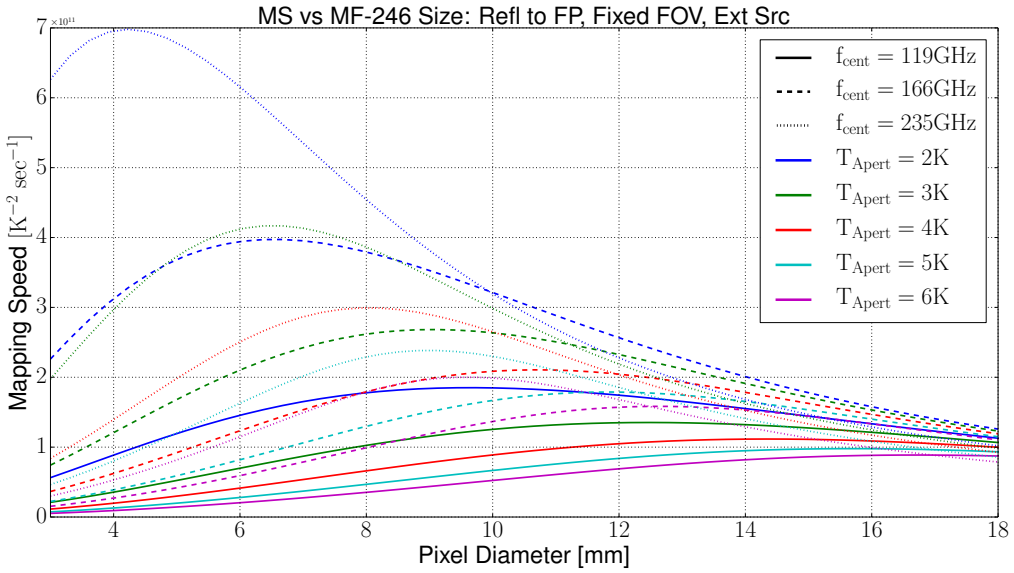

Figure 31: MF-246 mapping speed of an extended source as a function of pixel diameter for cold reflections and fixed FOV

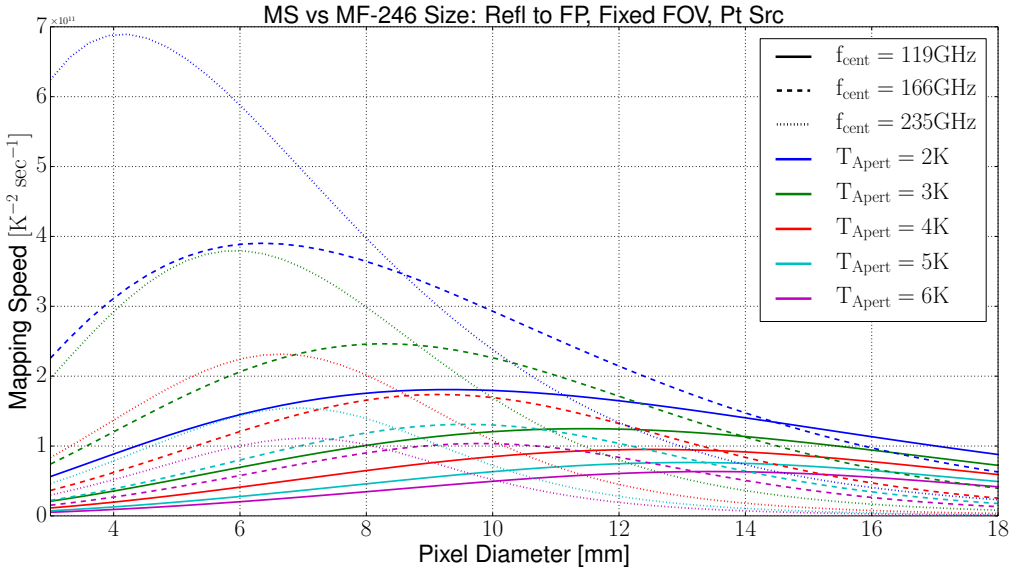

Figure 32: MF-246 mapping speed of a point source as a function of pixel diameter for cold reflections and fixed FOV

8.3.5 HFT

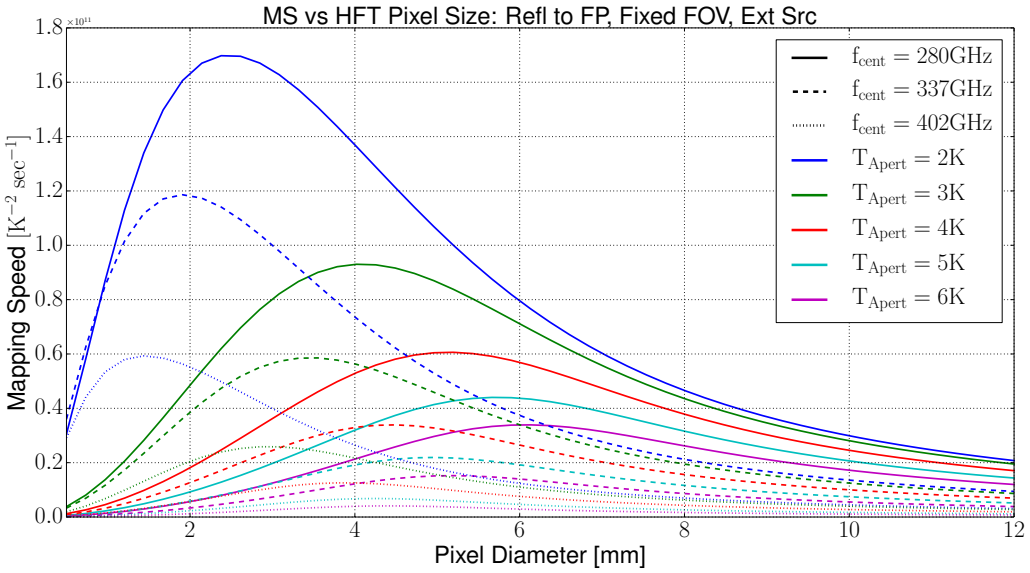

Figure 33: HFT mapping speed of an extended source as a function of pixel diameter for cold reflections and fixed FOV

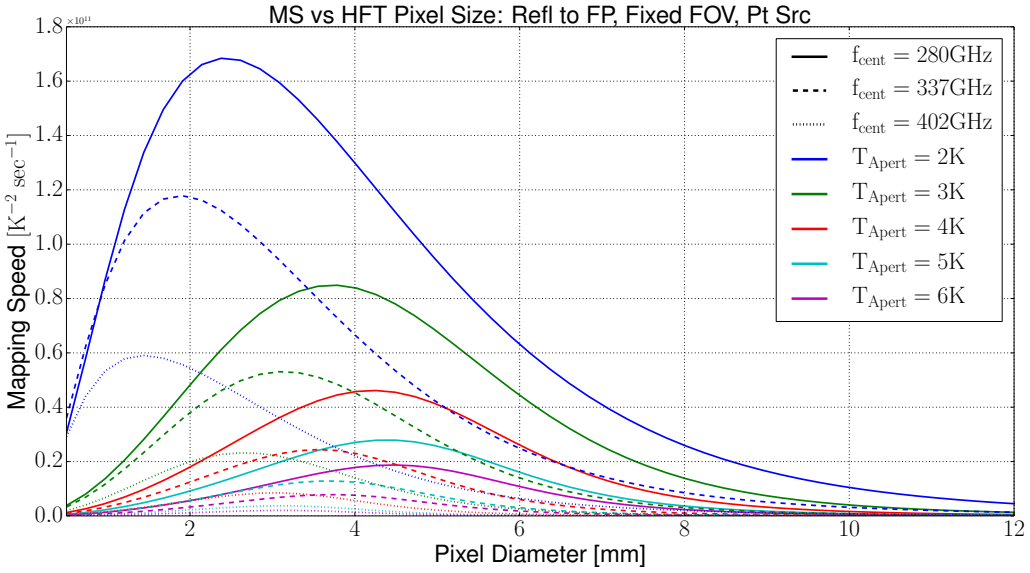

Figure 34: HFT mapping speed of a point source as a function of pixel diameter for cold reflections and fixed FOV

8.4 Reflections Go to Focal Plane, Fixed Number of Detectors

This subsection containts the results for the optimization of pixel diameters for the LFT and HFT given a fixed number of detectors and assuming all reflections go back to the focal plane.

8.4.1 LF-135

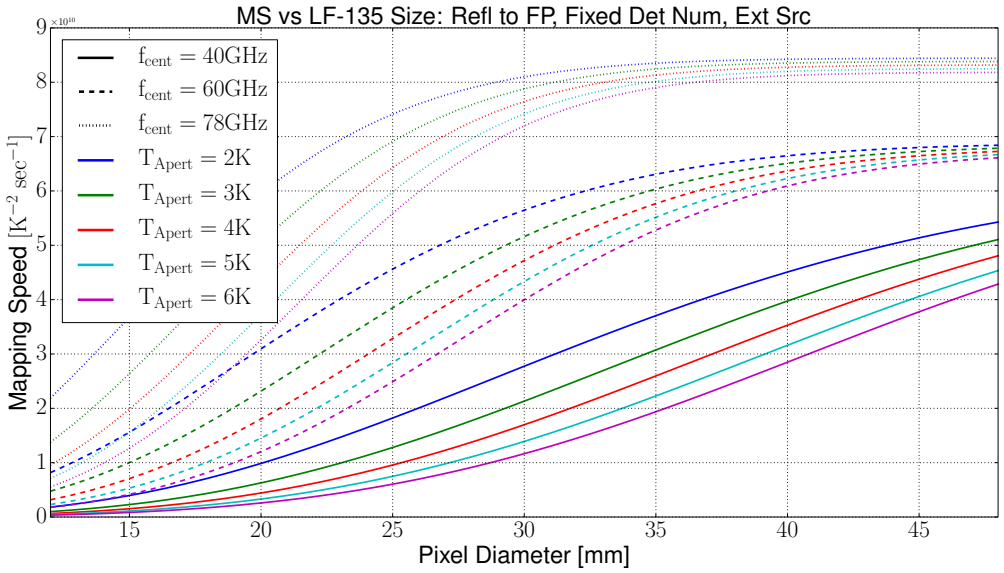

Figure 35: LF-135 mapping speed of an extended source as a function of pixel diameter for cold reflections and fixed number of detectors

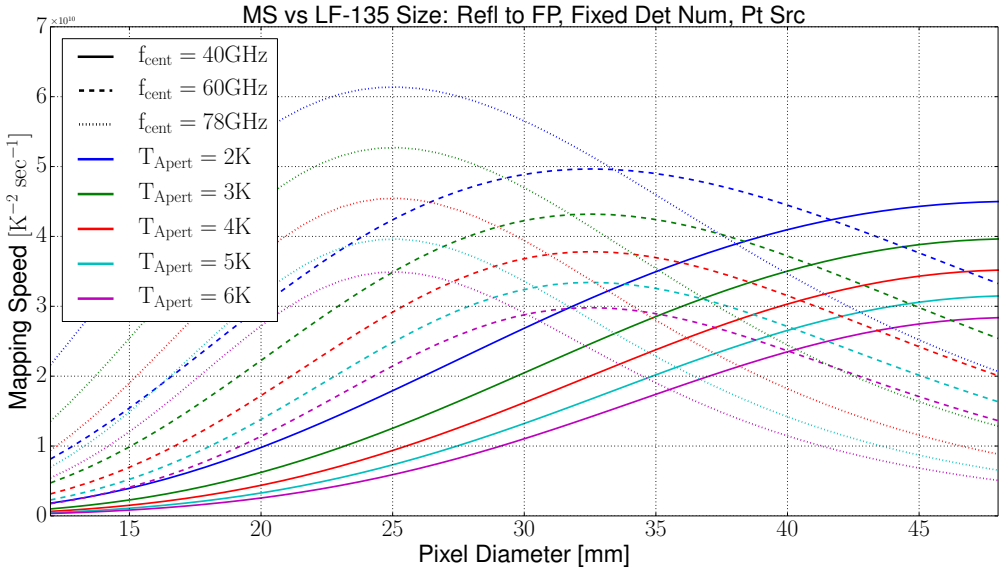

Figure 36: LF-135 mapping speed of a point source as a function of pixel diameter for cold reflections and fixed number of detectors

8.4.2 LF-246

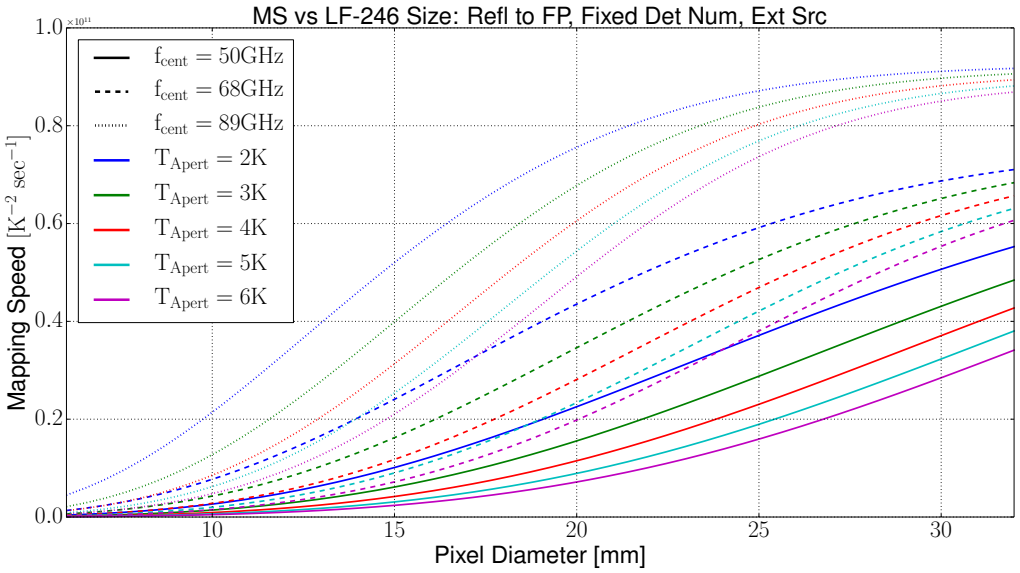

Figure 37: LF-246 mapping speed of an extended source as a function of pixel diameter for cold reflections and fixed number of detectors

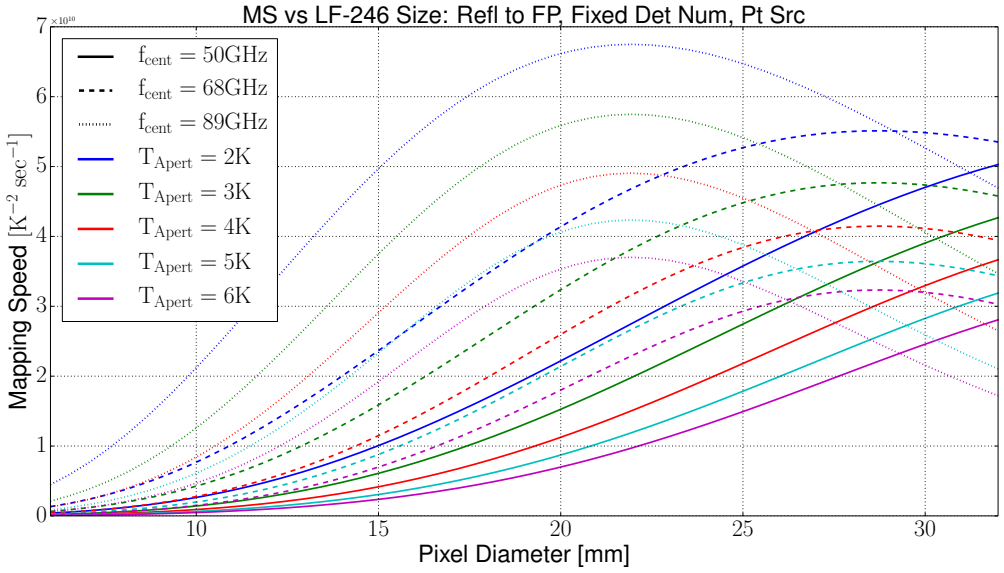

Figure 38: LF-246 mapping speed of a point source as a function of pixel diameter for cold reflections and fixed number of detectors

8.4.3 MF-135

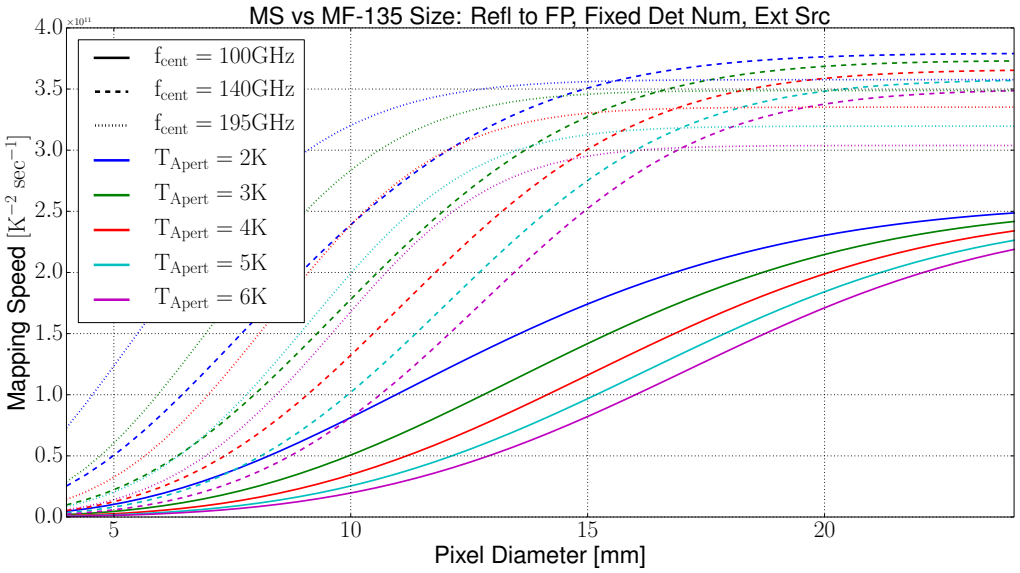

Figure 39: MF-135 mapping speed of an extended source as a function of pixel diameter for cold reflections and fixed number of detectors

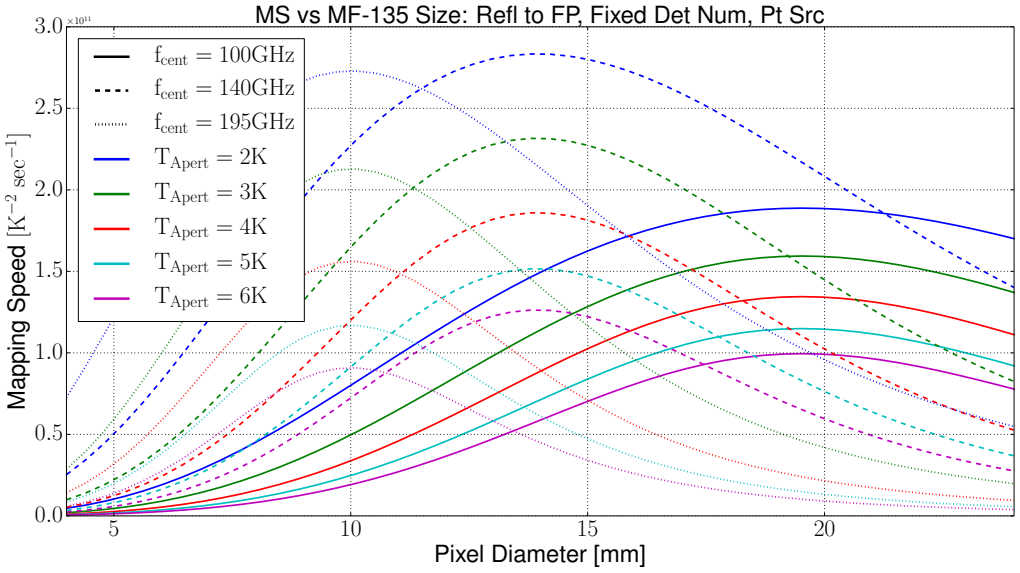

Figure 40: MF-135 mapping speed of a point source as a function of pixel diameter for cold reflections and fixed number of detectors

8.4.4 MF-246

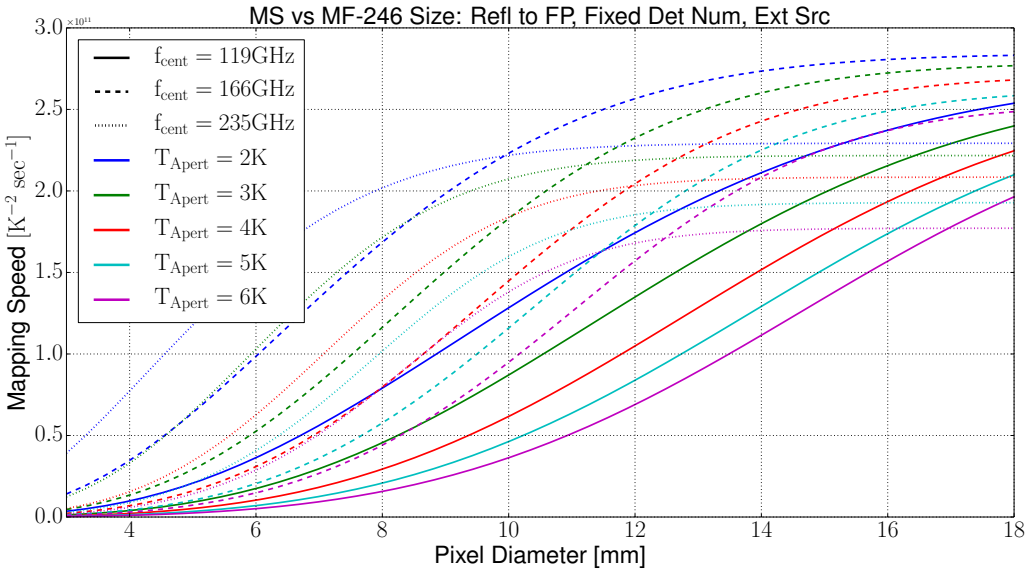

Figure 41: MF-246 mapping speed of an extended source as a function of pixel diameter for cold reflections and fixed number of detectors

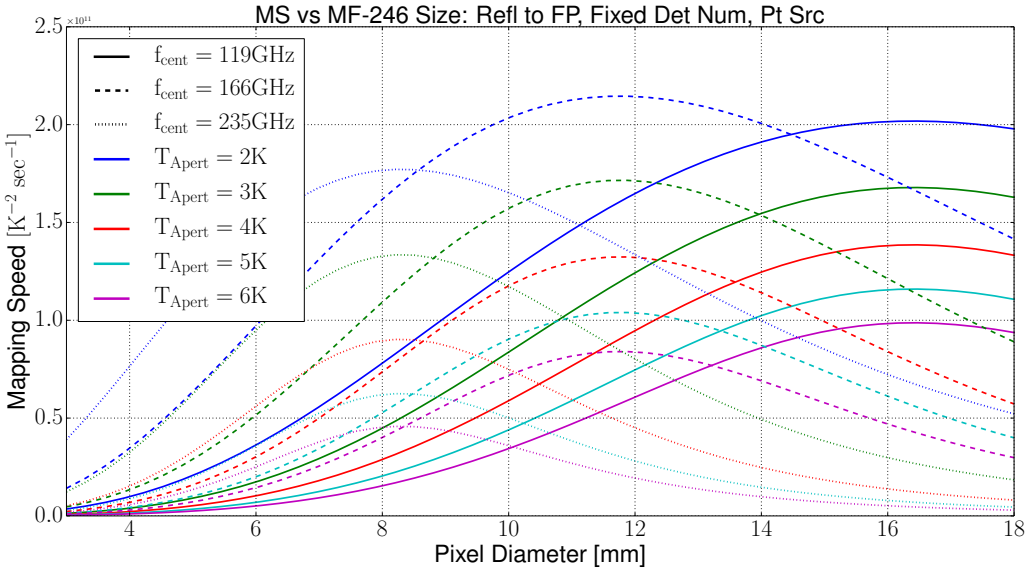

Figure 42: MF-246 mapping speed of a point source as a function of pixel diameter for cold reflections and fixed number of detectors

8.4.5 HFT

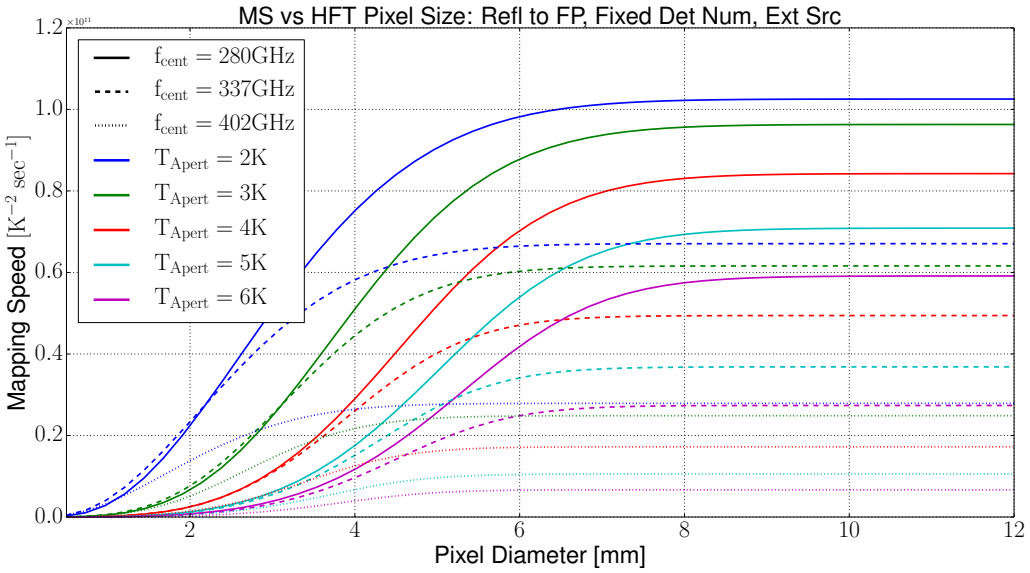

Figure 43: HFT mapping speed of an extended source as a function of pixel diameter for cold reflections and fixed number of detectors

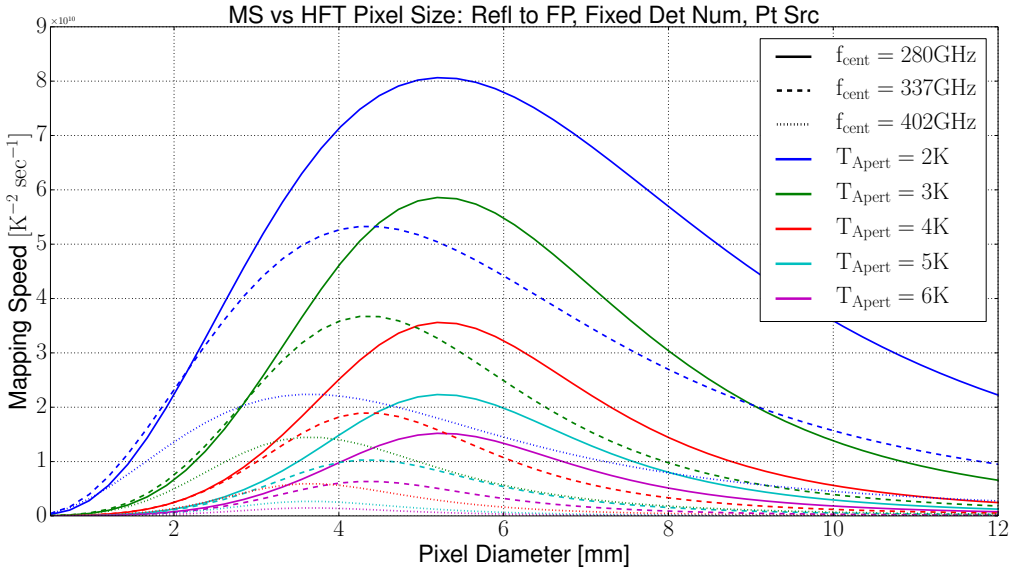

Figure 44: HFT mapping speed of a point source as a function of pixel diameter for cold reflections and fixed number of detectors

8.5 Summary of Optimal Diameters

Table 29 describes the assumptions that we take in this document when identifying the optimal pixel diameters for each frequency channel.

Parameter	Assumed Value	Comment
Baffle Temperature	5 K	Helium-cooled
Aperture Temperature	5 K	Helium-cooled
Focal Plane Limitation	FOV-limited	Cannot push Strehl's, payload, fabrication cost, etc
Reflections	Land on baffle	Most conservative assumption
Observation Source	Extended	We are primarily interested in the CMB

Table 29: Assumptions behind finding optimal pixel diameters

NOTE THAT THE OPTIMAL PIXEL DIAMETERS LAYED OUT IN THIS SECTION ARE LEFTOVER FROM BEFORE THE BAFFLE MOVED TO 2 K AND THEREFORE SHOULD BE UPDATED. We may be in a regime where we are readout-limited, but if not, then we can perhaps pack more detectors onto the focal plane using smaller pixel diameters for enhanced mapping speed.

Given these assumptions in the above table, Table 30 shows the optimal pixel diameter for each frequency channel.

Because we have three channels on each triplexed pixel, it is prudent to choose one frequency to favor over the other two. For this analysis, we aim to maximize sensitivity on the channels that receive the most CMB power. I've boldfaced the frequency channel that I think should determine the each pixel's diameter.

Band	Optimal Pixel Diameter [mm]
LF-135	
LF-1	37.0
LF-3	24.5
LF-5	**19.4**
LF-246	
LF-2	29.9
LF-4	21.9
LF-6	**16.6**
MF-135	
MF-1	15.0
MF-3	**10.9**
MF-5	8.1
MF-246	
MF-2	12.8
MF-4	**9.4**
MF-6	6.7
HFT	
HF-1	**4.3**
HF-2	**3.6**
HF-3	**3.1**

Table 30: Summary of optimal pixel diameters

8.6 Choosing Pixel Diameters

Given the discussion of Section 8.5, we now must choose our pixel diameters. There are a few considerations whe making this decision:

1. Quantization of hexagonal wafer division
2. Minimum allowed diameter for the lowest frequency channel on each pixel
3. Maximum allowed diameter given a finite wafer size and number of pixels on that wafer

We will take a brief look at all of these considerations in the following sections.

8.6.1 Hexagon Quantization and Maximum Pixel Diameter

Assuming a 110mm hexagonal wafer, Figure 45 shows the allowed pixel configurations, their pixel count, and the maximum allowed pixel diameter allowed by that configuration.

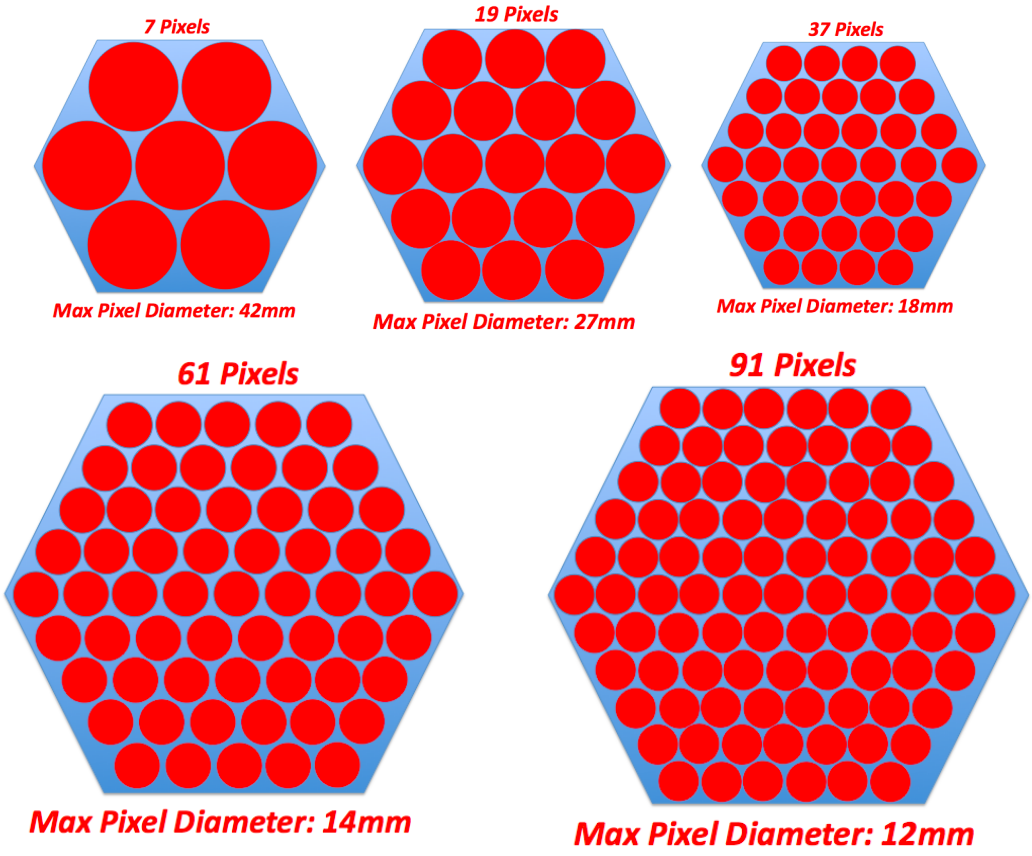

Figure 45: Allowed pixel configurations and their maximum allowed diameters assuming that the host wafer is 110mm side-to-side

8.7 Lenslet Focusing and Minimum Pixel Diameter

In order for a lenslet to have adequate focusing power, its diameter needs to obey the relation

$$D \geq 2\,\lambda_0 \tag{33}$$

where λ_0 is the wavelength of the incident radiation in a vacuum. Given this constraint, we can set a lower bound on the allowed diameter of each pixel by considering the lowest edge of its lowest frequency band.

Note that these minimum values only apply to LFT pixels.

Pixel	Lowest Frequency [GHz]	Minimum Diameter [mm]
LF-135	34	18
LF-246	43	14
MF-135	85	7.1
MF-246	101	5.9

Table 31: Minimum allowed diameters for LFT pixels

8.8 Pixel Diameters for this Document

Given the constraints laid out in this section, we take the pixel diameters listed in Table 32.

Pixel	Diameter [mm]
LF-135	18
LF-246	18
MF-135	12
MF-246	12
HF-1	5.4
HF-2	4.5
HF-3	4.0

Table 32: Pixel sizes used in this document

Note that at the lower frequencies, the mapping speed is a slower function of pixel diameter than at higher frequencies. Therefore, we don't suffer so much by deploying the LF pixels below optimal diameter.

9 Discussions

NOTE: These studies are old and need to be updated to take a 2 K aperture into account.

This is the "grab bag" section that includes topics not directly related to the sensitivity calculation.

9.1 Range of Possible Optical Loading

It is important to understand the range of optical loading values that lie withint the realm of possibility for LiteBIRD. According to the assertions in this document, the "extreme" scenarios (code name "S#"), listed from smallest expected photon loading to largest, are

S1: Reflections to focal plane, 4.5K baffling temperature

S2: Reflections to baffling, 4.5K baffling temperature

S3: Reflections to focal plane, 6.0K baffling temperature

S4: Reflections to baffling, 6.0K baffling temperature

In Table 33, we list the in-band loading values for every frequency channel in each of the above scenarios.

Band	P_{opt} [pW]			
	S1	S2	S3	S4
LF-1	0.32	0.33	0.43	0.44
LF-2	0.34	0.36	0.46	0.48
LF-3	0.27	0.29	0.35	0.38
LF-4	0.26	0.29	0.34	0.38
LF-5	0.25	0.29	0.32	0.36
LF-6	0.24	0.28	0.29	0.35
MF-1	0.31	0.34	0.42	0.46
MF-2	0.35	0.40	0.46	0.54
MF-3	0.29	0.35	0.37	0.47
MF-4	0.22	0.29	0.27	0.39
MF-5	0.17	0.24	0.20	0.32
MF-6	0.12	0.18	0.14	0.26
HF-1	0.12	0.15	0.19	0.26
HF-2	0.08	0.11	0.16	0.22
HF-3	0.04	0.05	0.08	0.12

Table 33: In-band loading for extreme scenarios

In Table 34, we list the photon noise values for every frequency channel in each of the above scenarios.

Band	NEP_{ph} [aW/$\sqrt{Hz}$]			
	S1	S2	S3	S4
LF-1	5.82	5.97	7.31	7.51
LF-2	6.20	6.43	7.61	7.94
LF-3	5.63	5.92	6.75	7.15
LF-4	5.72	6.08	6.72	7.22
LF-5	5.77	6.22	6.61	7.24
LF-6	5.78	6.32	6.45	7.23
MF-1	6.97	7.38	8.36	8.94
MF-2	7.85	8.48	9.20	10.1
MF-3	7.57	8.38	8.63	9.85
MF-4	7.13	8.15	7.88	9.50
MF-5	6.64	7.87	7.17	9.22
MF-6	6.04	7.47	6.51	9.04
HF-1	6.73	7.54	8.47	9.90
HF-2	6.03	6.86	8.30	9.81
HF-3	4.34	5.07	6.60	8.00

Table 34: Photon noise for extreme scenarios

9.2 Effect of Optical Element Temperatures on Sensitivity

The following plots show the effect of the temperature of the optical elements shown in Table 35 on LB sensitivity, both band-by-band and for the instrumet as a whole.

Optical Element	Temperature Range [K]
Baffle	4.5 - 6.5
HWP	4.5 - 6.5
Aperture	4.5 - 6.5
Mirrors (LFT)/Lenses (HFT)	4.5 - 6.5

Table 35: Optical elements whose temperature depends on 4K fridge performance

9.2.1 Effect of Baffle Temperature

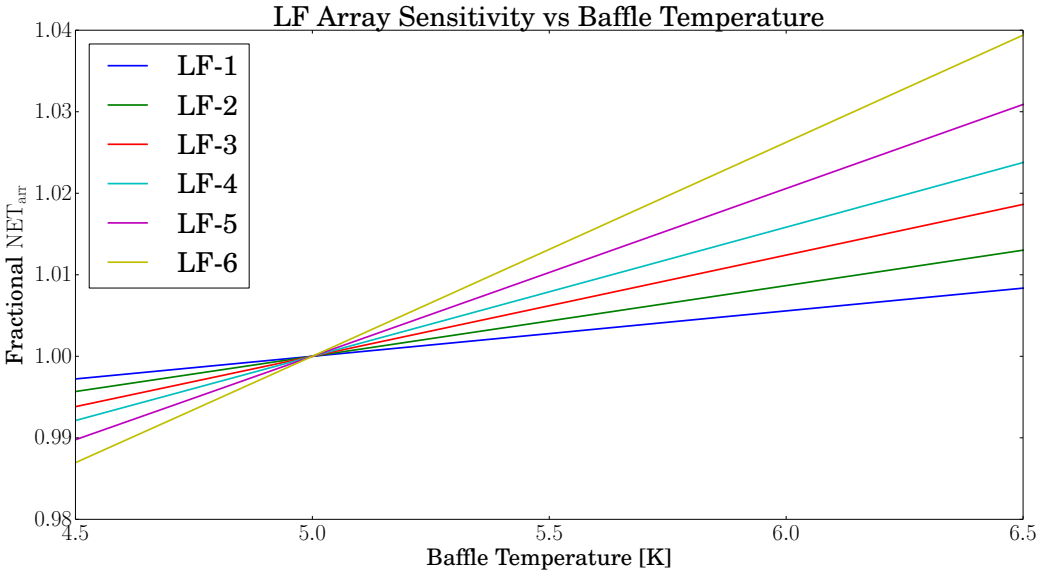

Figure 46: LF Array sensitivity vs Baffle temperature

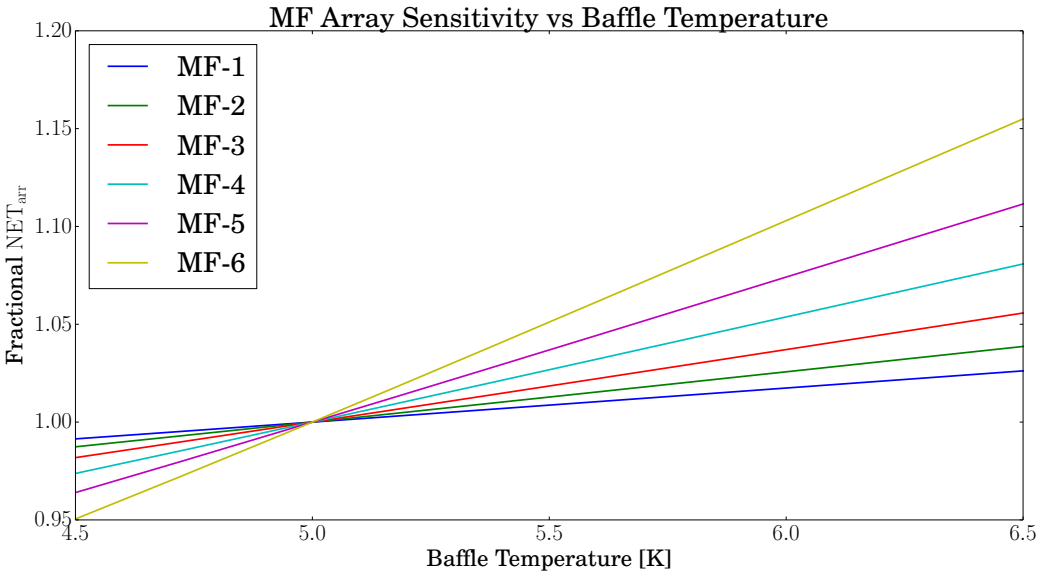

Figure 47: MF Array sensitivity vs Baffle temperature

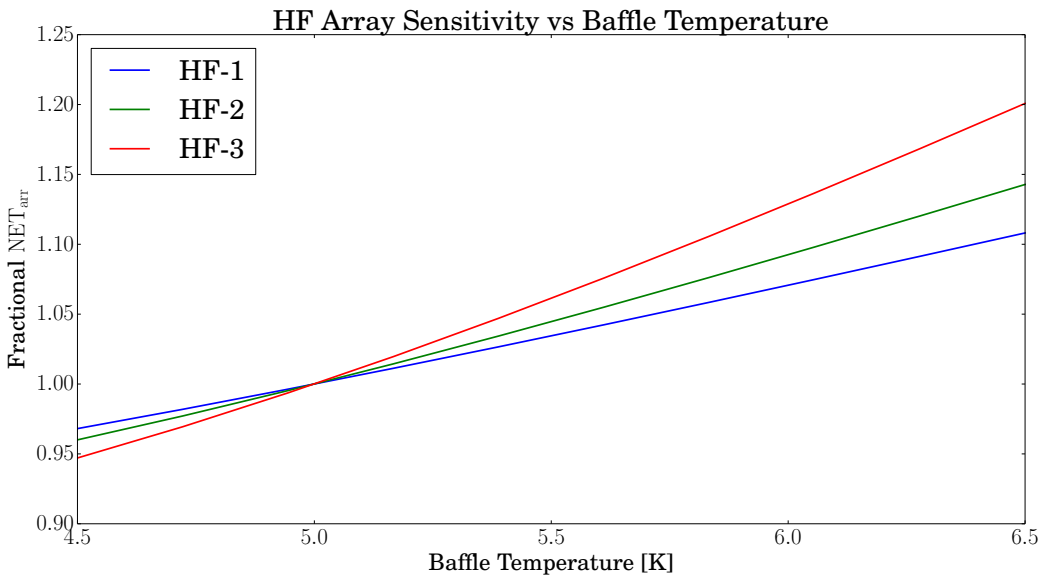

Figure 48: HF Array sensitivity vs Baffle temperature

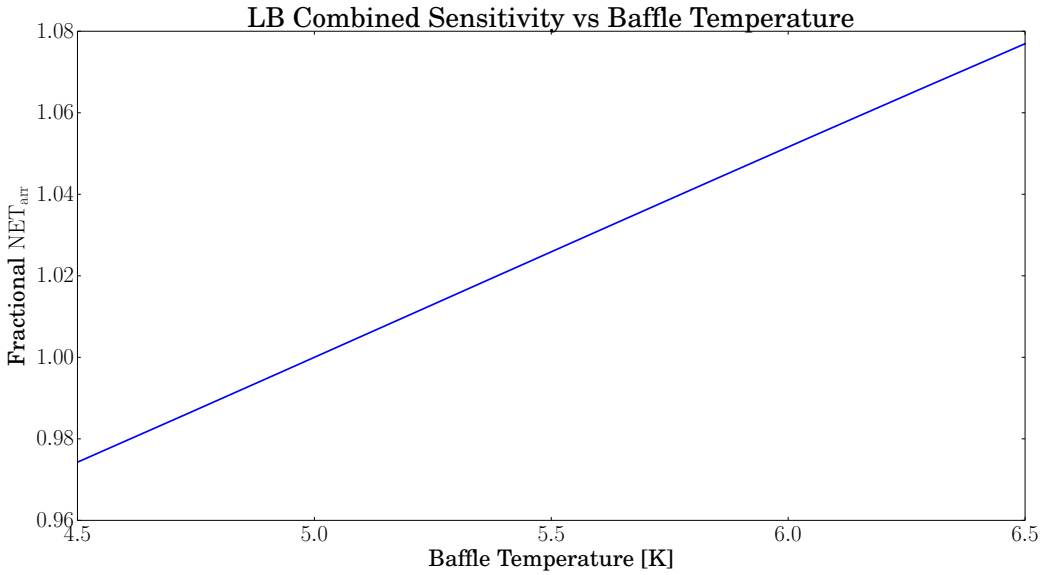

Figure 49: LB sensitivity vs Baffle temperature

9.2.2 Effect of HWP Temperature

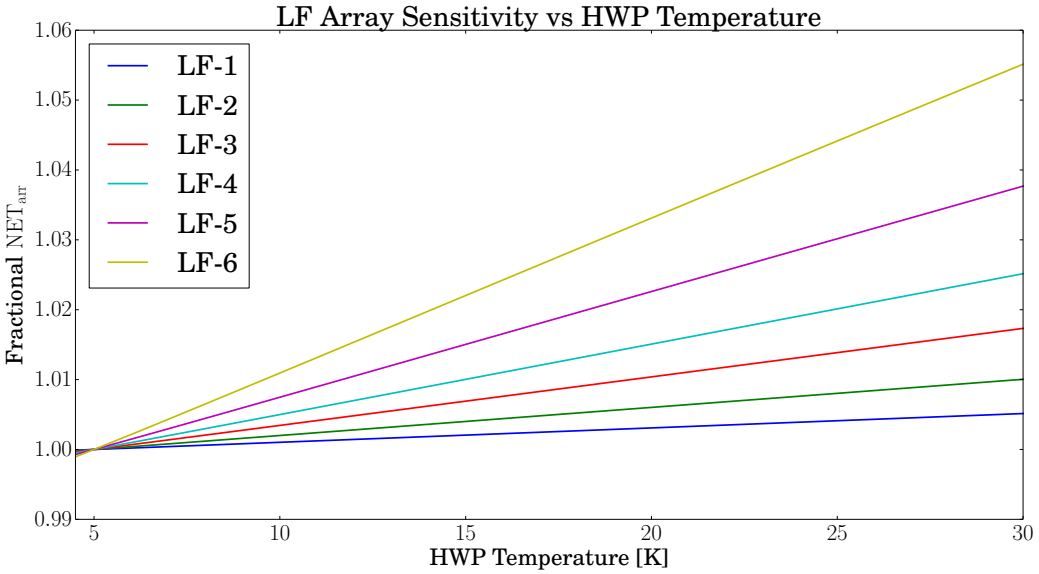

Figure 50: LF Array sensitivity vs HWP temperature

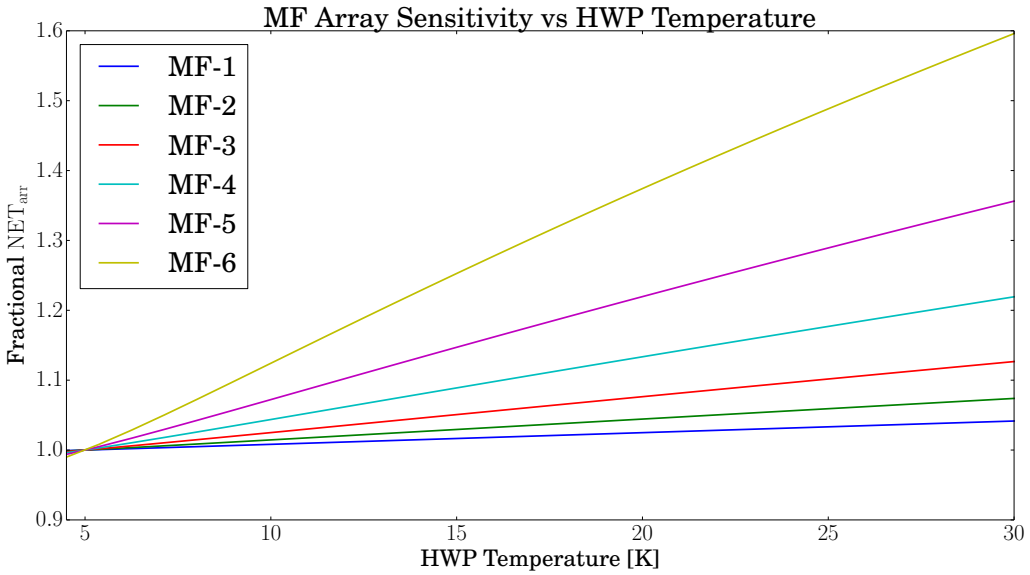

Figure 51: MF Array sensitivity vs HWP temperature

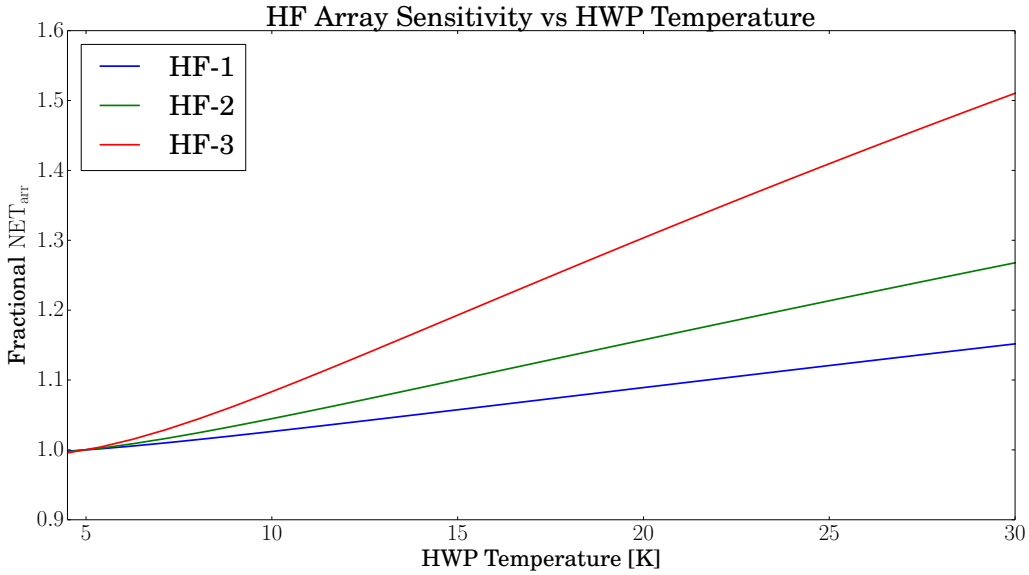

Figure 52: HF Array sensitivity vs HWP temperature

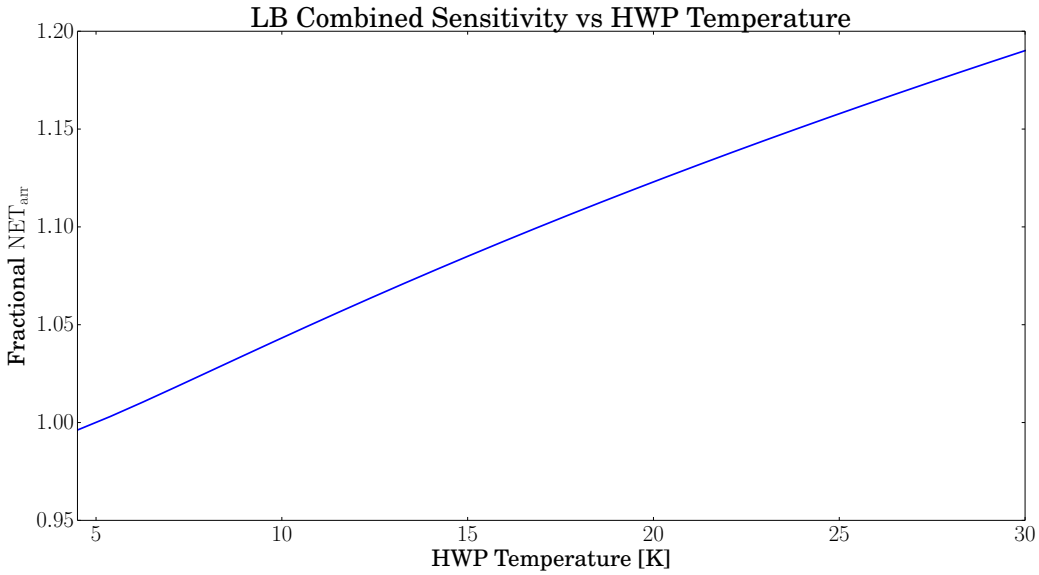

Figure 53: LB sensitivity vs HWP temperature

9.2.3 Effect of Aperture Temperature

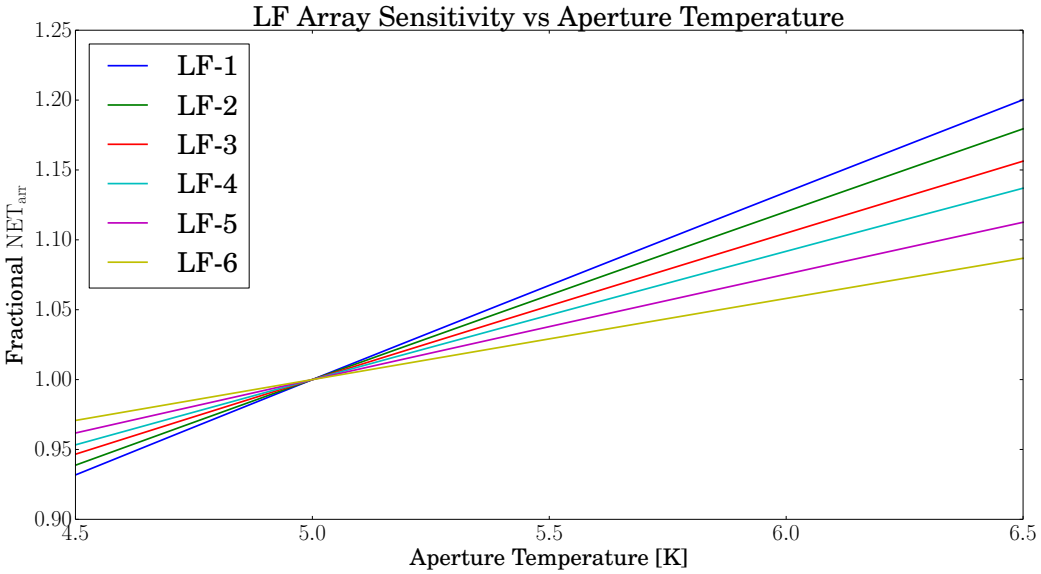

Figure 54: LF Array sensitivity vs Aperture temperature

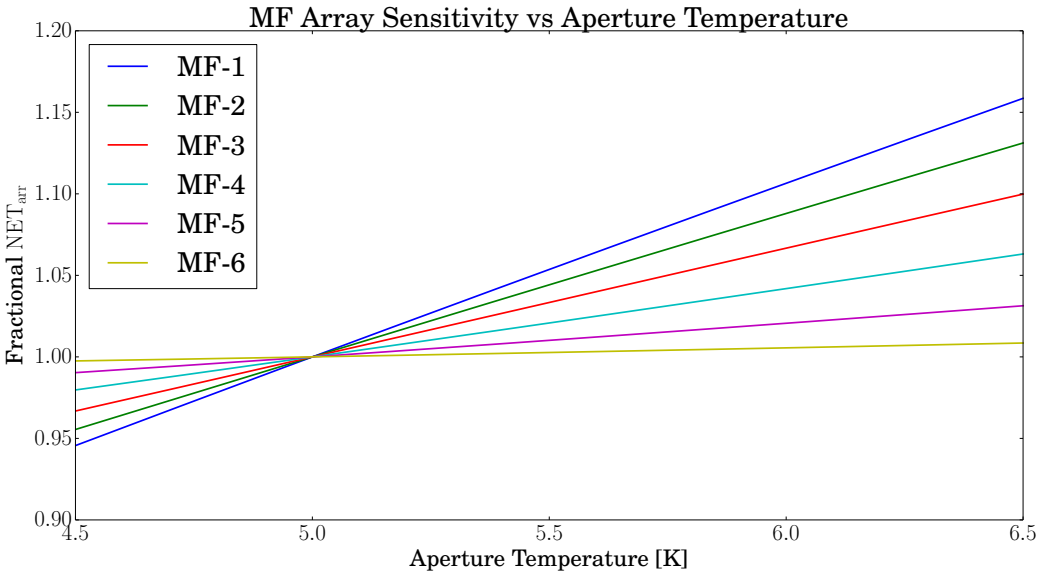

Figure 55: MF Array sensitivity vs Aperture temperature

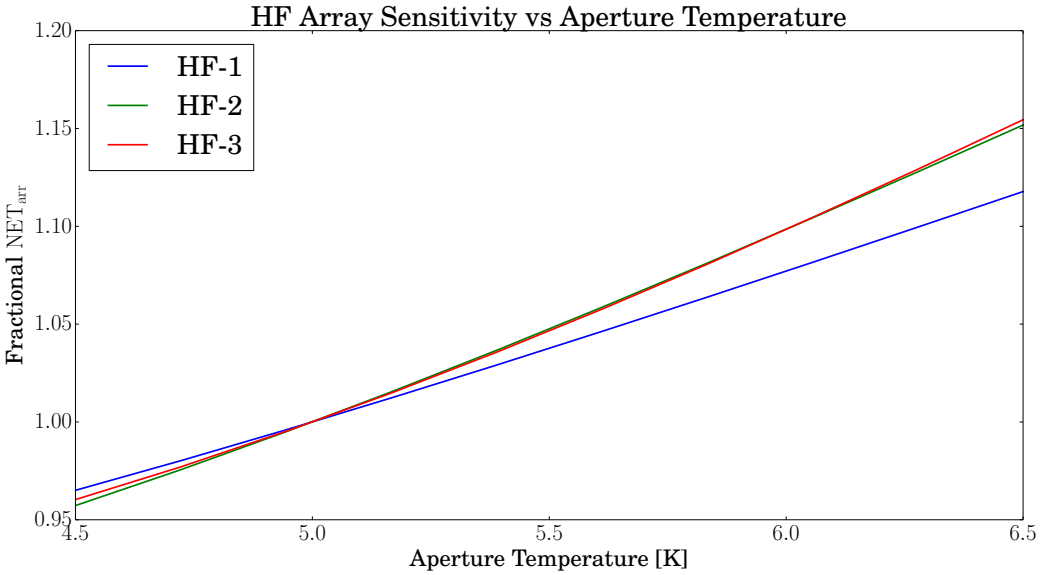

Figure 56: HF Array sensitivity vs Aperture temperature

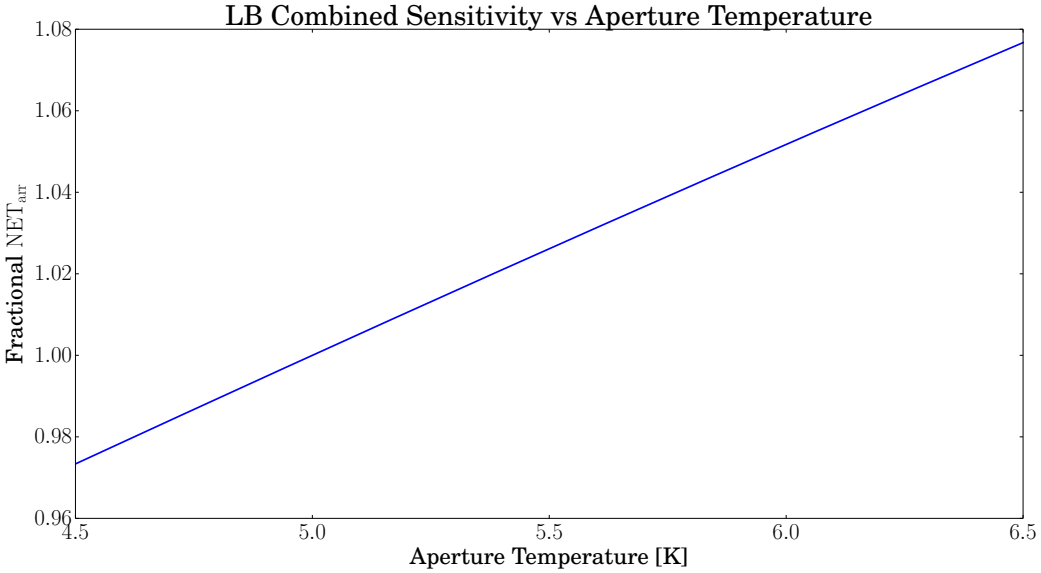

Figure 57: LB sensitivity vs Aperture temperature

9.2.4 Effect of Mirror/Lens Temperature

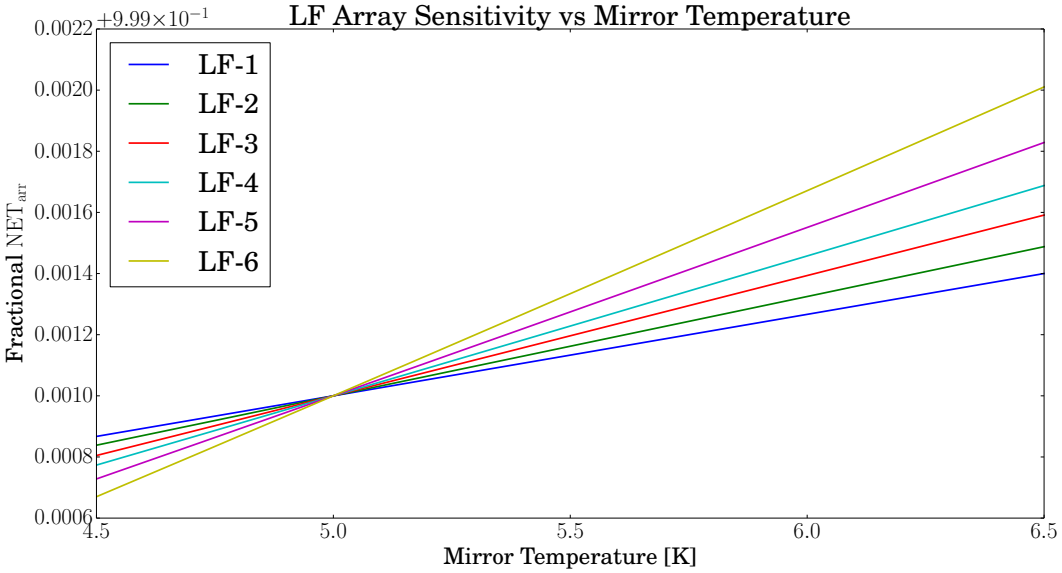

Figure 58: LF Array sensitivity vs Mirror temperature

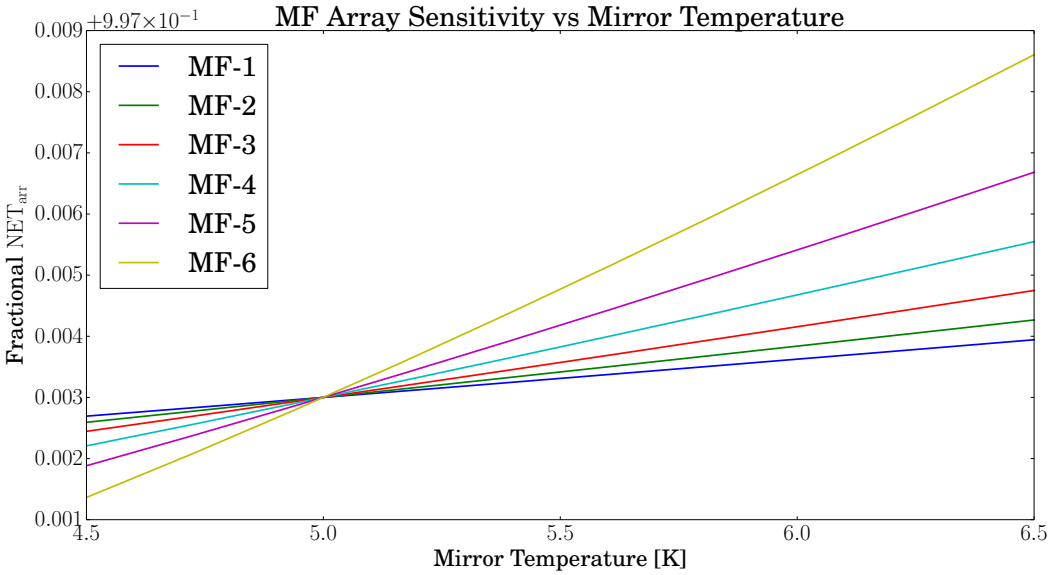

Figure 59: MF Array sensitivity vs Mirror temperature

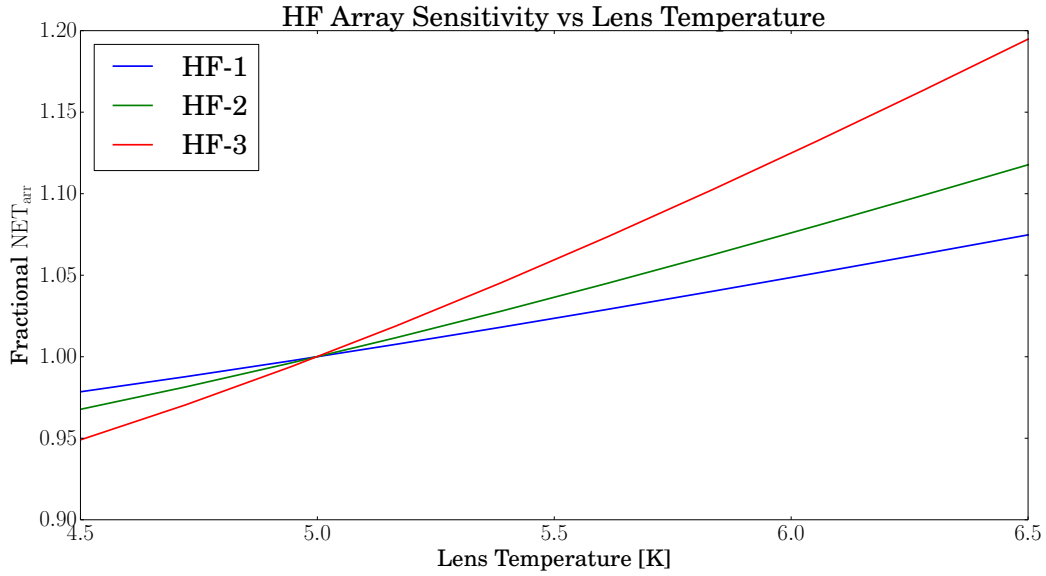

Figure 60: HF Array sensitivity vs Lens temperature

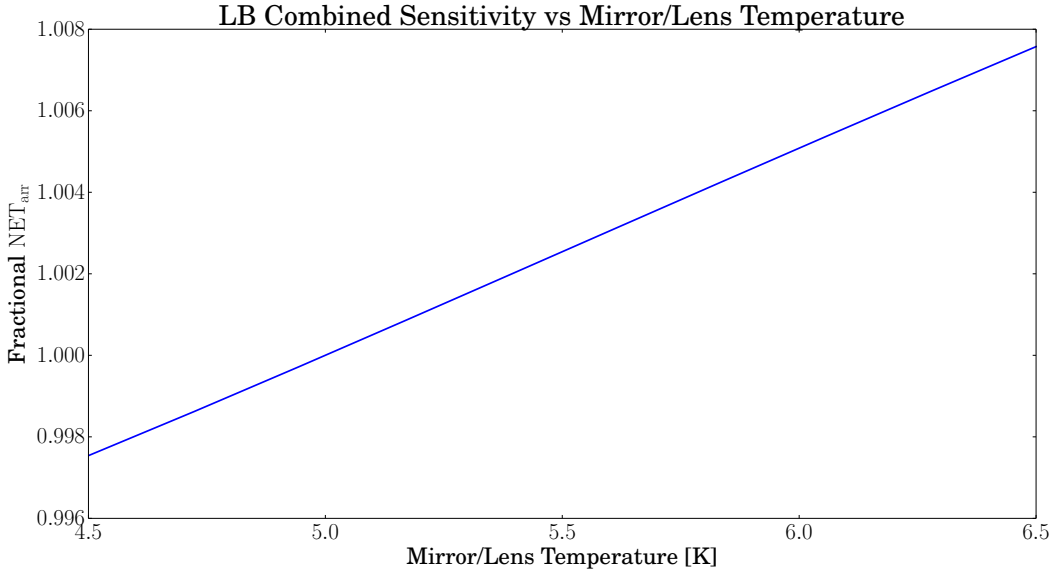

Figure 61: LB sensitivity vs Mirror/Lens temperature

9.3 Still To Do

There are still many tasks to complete before this analysis can be taken seriously. This list of tasks includes

1. Estimate external noise $\mathrm{NEP}_{\mathrm{ext}}$ for each frequency channel
2. Critically evaluate the sensitivity contingency we're giving ourselves, given all these possible sources and how much/little we know about them
3. ...

References

[1] V. V. Parshin et al. *Silicon as an Advanced Window Material for High Power Gyrotrons.* http://link.springer.com/article/10.1007\%2FBF02066662

[2] James W. Lamb. *Miscellaneous Data on Materials for Millimetre and Submillimetre Optics* http://link.springer.com/article/10.1007\%2FBF02069487

[3] W. Kasparek et al. *Measurements of Ohmic Losses of Metallic Reflectors at 140 GHz Using a 3-Mirror Resonator Technique* http://link.springer.com/article/10.1023\%2FA\%3A1015064616703

[4] Peter Ade at al. *A Review of Metal Mesh Filters* http://asd.gsfc.nasa.gov/cosmology/spirit/tech_papers/Ade_filter_review.pdf

[5] Aritoki Suzuki *350mK Metal Mesh Filter Band Pass Filter Analysis* https://bolowiki.berkeley.edu/twiki/bin/view/Main/PB2350mKMetalMeshBandAnalysis

[6] S. Roose et al. *Design of the cryo-optical test of the Planck Reflectors* https://orbi.ulg.ac.be/bitstream/2268/82057/1/cryo-optical\%20test\%20of\%20the\%20planck\%20reflectors.pdf

[7] Aritoki Suzuki. *Multichroic Detector Architecture for Cosmic Microwave Background Polarimetry Experiments* http://search.proquest.com/docview/1526024558

[8] Kam Arnold. *Design and Deployment of the Polarbear Cosmic Microwave BackgroundPolarization Experiment* http://escholarship.org/uc/item/99m8b32x\#page-1

[9] Jonas Zmuidzinas. *Thermal noise and correlations in photon detection* http://www.submm.caltech.edu/~jonas/tex/papers/pdf/2003-APPLOPT-Zmuidzinas.pdf

[10] Brian Keating. *BICEP: A Large Angular Scale CMB Polarimeter* http://bicep0.caltech.edu/public/bicep/BICEP_color.pdf

[11] A. Baryshev, W. Wild. *ALMA Band 9 Optical Layout.* http://legacy.nrao.edu/alma/memos/html-memos/alma394/memo394.pdf